# Atmospheric reactivity and oxidation capacity during summer at a suburban site between Beijing and Tianjin

Yuan Yang[1,2], Yonghong Wang[3], Putian Zhou[3,4], Dan Yao[1,2,5], Dongsheng Ji[1], Jie Sun[1], Yinghong Wang[1], Shuman Zhao[1,2], Wei Huang[1,2], Shuanghong Yang[1,5], Dean Chen[3], Wenkang Gao[1], Zirui Liu[1], Bo Hu[1], Renjian Zhang[1], Limin Zeng[6], Maofa Ge[7], Tuukka Petäjä[3], Veli-Matti Kerminen[3], Markku Kulmala[3], Yuesi Wang[1,2,8]

[1] Institute of Atmospheric Physics, Chinese Academy of Sciences, Beijing 100029, China

[2] University of the Chinese Academy of Sciences, Beijing 100049, China

[3] Institute for Atmospheric and Earth System Research / Physics, Faculty of Science, P.O.Box 64, 00014 University of Helsinki, Helsinki, Finland

[4]Climate and Marine Sciences Department, Eurasia Institute of Earth Sciences, Istanbul Technical University, Maslak 34469, Istanbul, Turkey

[5]Department of Environmental Science and Engineering, Beijing University of Chemical Technology, Beijing 10029, China

[6]State Joint Key Laboratory of Environmental Simulation and Pollution Control, College of Environmental Sciences and Engineering, Peking University, Beijing 100871, China

[7] State Key Laboratory for Structural Chemistry of Unstable and Stable Species, CAS Research/Education Center for Excellence in Molecular Sciences, Institute of Chemistry, Chinese Academy of Sciences, Beijing 100190, China

[8] Center for Excellence in Regional Atmospheric Environment, Institute of Urban Environment, Chinese Academy of Sciences, Xiamen 361021, China

Revised to: Atmospheric Chemistry and Physics

Corresponding to: Yonghong Wang, yonghong.wang@helsinki.fi; Yuesi Wang, wys@mail.iap.ac.cn

**Abstract**

Hydroxyl (OH) radicals, nitrate ($NO_3$) radicals, and ozone ($O_3$) play central roles in the troposphere because they control the lifetimes of many trace gases that result from anthropogenic and biogenic origins. To estimate the air chemistry, the atmospheric reactivity and oxidation capacity were comprehensively analyzed based on a parameterization method at a suburban site in Xianghe in the North China Plain from 6 July 2018 to 6 August 2018. The total OH, $NO_3$ and $O_3$ reactivities at the site varied from 9.2 $s^{-1}$ to 69.6 $s^{-1}$, 0.7 $s^{-1}$ to 27.5 $s^{-1}$ and $3.3\times10^{-4}$ $s^{-1}$ to $1.8\times10^{-2}$ $s^{-1}$ with campaign-averaged values of 27.5±9.7 $s^{-1}$, 2.2±2.6 $s^{-1}$ and $1.2\pm1.7\times10^{-3}$ $s^{-1}$ (± standard deviation), respectively. $NO_x$ ($NO+NO_2$) was by far the main contributor to the reactivities of the three oxidants, with average values of 43-99%. Alkenes dominated the OH, $NO_3$ and $O_3$ reactivities towards total nonmethane volatile organic compounds (NMVOCs), accounting for 42.9%, 77.8% and 94.0%, respectively. The total OH, $NO_3$ and $O_3$ reactivities displayed similar diurnal variations with the lowest values during the afternoon but the highest values during rush hours, and the diurnal profile of $NO_x$ appears to be the major driver for the diurnal profiles of the reactivities of the three oxidants. A box model (a model to Simulate the concentrations of Organic vapors, Sulfuric Acid and Aerosols, SOSAA) derived from a column chemical transport model was used to simulate OH and $NO_3$ concentrations during the observation period. The calculated atmospheric oxidation capacity (AOC) reached $4.5\times10^{8}$ molecules $cm^{-3}$ $s^{-1}$ with a campaign-averaged value of $7.8\times10^{7}$ molecules $cm^{-3}$ $s^{-1}$ dominated by OH ($7.7\times10^{7}$ molecules $cm^{-3}$ $s^{-1}$, 98.2%), $O_3$ ($1.2\times10^{6}$ molecules $cm^{-3}$ $s^{-1}$, 1.5%) and $NO_3$ ($1.8\times10^{5}$ molecules $cm^{-3}$ $s^{-1}$, 0.3%). Overall, the integration of OH, $NO_3$ and $O_3$ reactivity analysis could provide useful insights for NMVOCs pollution control in the North China Plain. We suggest that further studies, especially direct observations of OH and $NO_3$ radical concentrations and their reactivities, are required to better understand trace gas reactivity and AOC.

**Keywords:**

VOCs, atmospheric oxidant reactivity, atmospheric oxidation capacity, North China Plain

## 1 Introduction

In the planetary boundary layer, high concentrations of primary pollutants, such as carbon monoxide (CO), nitrogen oxides ($NO_x$=$NO+NO_2$) and volatile organic compounds (VOCs) from

both biogenic and anthropogenic origins, are transformed by reactions with atmospheric oxidants, such as hydroxyl (OH) radicals, nitrate ($NO_3$) radicals, chlorine atoms and ozone ($O_3$) on local to global scales (Atkinson and Arey, 2003;Heard and Pilling, 2003;Lu et al., 2018;Wang et al., 2020), with the dominant reaction depending on the time of day and specific trace gases. Ultimately, these processes lead to the formation of a series of important secondary pollutants, including tropospheric $O_3$ and secondary organic aerosols (SOA) (Goldstein and Galbally, 2007).

OH radicals control the daytime oxidation capacity of the atmosphere (Heard and Pilling, 2003), initiating and participating in many oxidation reaction processes. OH can react by adding OH groups to or abstracting H from trace gases, such as CO, $NO_x$, methane ($CH_4$), nonmethane volatile organic compounds (NMVOCs) (Kovacs et al., 2003;Sadanaga et al., 2005). The total OH reactivity, which is equivalent to the inverse chemical OH lifetime, is the sum of the products of the concentrations and respective reaction rate coefficients for all gases that react with OH. The online techniques used to determine OH reactivity include a flow tube with sliding injector method (Kovacs et al., 2003), a comparative rate method (Sinha et al., 2008) and a laser flash photolysis pump probe technique (Whalley et al., 2016). Based on these online methods, total OH reactivity values have been measured in urban, suburban, remote and forest areas during the last decade. The urban areas investigated include Nashville, USA (SOS) (Kovacs et al., 2003), New York, USA (PMTACS-NY2004) (Ren et al., 2006a), Mexico City, Mexico (MCMA-2003) (Shirley et al., 2006), Houston, USA (TRAMP2006) (Mao et al., 2010), Paris, France (MEGAPOLI) (Dolgorouky et al., 2012), London, UK (ClearfLo) (Whalley et al., 2016), Helsinki, Finland (Praplan et al., 2017), Seoul, South Korea (Kim et al., 2016) and Beijing, China (Yang et al., 2017). The total OH reactivity in these urban areas ranged from 1 $s^{-1}$ in clean air to 200 $s^{-1}$ in extremely polluted air, and $NO_x$, CO, formaldehyde (HCHO) and nonmethane hydrocarbons (NMHCs) were the main contributors (Ferracci et al., 2018). The suburban areas investigated include Whiteface Mountain, USA (PMTACS-NY2002) (Ren et al., 2006b), Weybourne, UK (TORCH-2) (Lee et al., 2010), Yufa, China (CAREBeijing-2006) (Lu et al., 2010), Backgarden, China (PRIDE-PRD) (Lou et al., 2010), Jülich, Germany (HOx Comp) (Elshorbany et al., 2012), Ersa, Corsica (CARBOSOR-ChArMeX) (Zannoni et al., 2017), Po Valley, Italy (Kaiser et al., 2015), the Indo-Gangetic Plain, India (Kumar et al., 2018) and Heshan, China (Yang et al., 2017). The total OH reactivity in these suburban areas

ranged from 4.6 to 64 $s^{-1}$. OH reactivity was also modeled by a global model by (Ferracci et al., 2018) and by a box model based on the Master Chemical Mechanism (MCM) (Whalley et al., 2016).The calculated total OH reactivity is the sum of the OH reactivities that are attributed to measured trace gases. The concentrations (in molecules $cm^{-3}$) of trace gases and the reaction rate constants (in $cm^3$ $molecule^{-1}$ $s^{-1}$) of these trace gases with the OH radical are the key factors for computing OH reactivity (Mogensen et al., 2011;Mogensen et al., 2015). In general, the trace gases considered in calculating OH reactivity include NMVOCs, $CH_4$, CO, $NO_x$, $SO_2$ and $O_3$. As reported, the contribution from $NO_x$ exceeds 50% for the cities of Paris, Tokyo, New York and Beijing, showing the large influence of traffic-related emissions on OH reactivity (Dolgorouky et al., 2012;Ren, 2003;Yang et al., 2017;Yoshino et al., 2006), but the contribution from NMVOCs reaches 50% in Mexico and Houston due to the large quantity of biomass fuel being burned and high industrial solvent emissions (Mao et al., 2010;Shirley et al., 2006).

As OH levels are vastly reduced during the nighttime due to the absence of photolysis, $NO_3$ formed by the slow reaction $NO_2 + O_3 \rightarrow NO_3 + O_2$ is the main initiator of nighttime oxidation chemistry in the troposphere (Asaf et al., 2009;Geyer et al., 2001). $NO_3$ reacts effectively with unsaturated NMVOCs, such as certain alkenes or aromatics via additions to >C=C< double bonds, which can initiate the formation of peroxyl radicals ($HO_2$ and $RO_2$) and even OH (Geyer et al., 2001). High $NO_3$ mixing ratios and large reaction rate constants with several unsaturated NMVOCs result in $NO_3$ being the dominant sink of many unsaturated NMVOCs during the nighttime. The role of $NO_3$ as an oxidizing agent can be assessed via its total reactivity towards trace gases. The total $NO_3$ reactivity is an indication of nighttime oxidation rates of trace gases with direct impacts on $NO_x$ levels and indirect impacts on heterogeneous $NO_x$ losses and $ClNO_2$ formation (Liebmann et al., 2017). As frequently reported for total OH reactivity, total $NO_3$ reactivity can be measured online or calculated by summing the loss rates for a set of reactive trace gases. Previous work on measured total $NO_3$ reactivity has revealed strong diel variation. For instance, the total $NO_3$ reactivity obtained in Hyytiälä, Finland, displayed strong diel variation, with a campaign-averaged nighttime value of 0.11 $s^{-1}$ and daytime value of 0.04 $s^{-1}$ (Liebmann et al., 2018a), but values varied from 0.005 to 0.1 $s^{-1}$ during the nighttime and reached values as high as 1.4 $s^{-1}$ in the daytime in Taunus, Germany (Liebmann et al., 2017).

Along with reactions with OH and $NO_3$ radicals, trace gases are also oxidized in the troposphere by reactions with $O_3$. Although most NMVOCs have reaction rates with $O_3$ that are much lower than those with either OH or $NO_3$, $O_3$ is very important because it is present at elevated mixing ratios in clean or contaminated atmospheres (Wang et al., 2013). The rate constants of the reactions for some alkenes with $O_3$ are even comparable to those with $NO_3$ (Atkinson and Arey, 2003). The total reactivity of $O_3$ with trace gases can reflect the role of $O_3$ as an oxidizing agent. Direct measurements of total $O_3$ reactivity were not available until very recently (Geyer, 2003); hence, the reactivity of $O_3$ has traditionally been calculated by summing the reactivities due to individual reactive trace gases. The calculated $O_3$ reactivity obtained in Pabstthum, Germany, revealed that terpenes (20%), isoprene (20%) and other alkenes (60%) were the dominant contributors during the night of 20 and 21 July but arose mainly (83%) from nonbiogenic alkenes during the night of 4 and 5 August (Geyer, 2003).

As mentioned above OH radicals, $NO_3$ radicals and $O_3$ react with trace gases via different rate coefficients and mechanisms, resulting in profoundly different reactivities. Therefore, comprehensive evaluations of OH, $NO_3$ and $O_3$ reactivities are key to understanding atmospheric oxidation capacity and identifying the controlling active species of secondary pollution in the atmosphere. However, comprehensive evaluations of the total calculated OH, $NO_3$ and $O_3$ reactivities are scarce in China. In this study, we calculated the OH, $O_3$ and $NO_3$ reactivities at a suburban site (Xianghe) in the North China Plain during an intensive measurement campaign in the summer of 2018. By combining simulated OH and $NO_3$ concentrations using a box model (a model to Simulate the concentrations of Organic vapors, Sulfuric Acid and Aerosols, SOSAA), we calculated the oxidation capacities of OH, $NO_3$ and $O_3$ and estimated their relative contributions.

## 2 Methodology

### 2.1 Site description

The sampling site is located at the Xianghe Atmospheric Observatory (39.798 °N, 116.958 °E; 15 m above sea level), which is operated by the Institute of Atmospheric Physics (IAP)/Chinese Academy of Sciences (CAS). The sampling site is a typical suburban site in the seriously polluted Beijing-Tianjin-Hebei large urban region, which is approximately 50 km southeast of Beijing, 75 km northwest of Tianjin, and 35 km northeast of Langfang in Hebei Province. The sampling site is

approximately 4 km west of the downtown center and is surrounded by residential areas and agricultural land (see Figure 1).

**2.2 Experimental method**

Ambient NMVOCs were collected and analyzed continuously and automatically with a time resolution of 1 h using a custom-built gas chromatography-mass spectrometry/flame ionization detector (GC-MS/FID) instrument. The suitability of this system for NMVOC measurements is well verified, and it has been used in several large field campaigns (Chen et al., 2014;Yuan et al., 2013;Wu et al., 2016). Detailed descriptions of the configuration of the GC-MS/FID system, the detection limits, and the precision of NMVOC measurements can be found in our previous paper (Yang et al., 2019). $CH_4$ was analyzed by an Agilent 7890A gas chromatography (GC) instrument with a flame ionization detector (FID). HCHO was measured by Hantzsch fluorimetry with a commercial instrument (AL4021, Aerolaser GmbH, Germany) (Lu et al., 2019). Air-quality-related trace gases, including $O_3$, NO-$NO_2$-NOx, $SO_2$ and CO were measured by analyzers from Thermo-Fisher Scientific, United States. High-resolution (5 min averages) data sets of $O_3$, NO, NO-$NO_2$-NOx, $SO_2$ and CO were obtained, and hourly averaged data were used after applying strict data quality control measures. HONO mixing ratios were determined using a custom-made HONO analyzer (Zhang et al., 2019;Tong et al., 2015). The photolysis frequencies, $JO^1D$, $JNO_2$ and $JNO_3$, in the atmosphere were measured by a PFS-100 photolysis spectrometer (Juguang Technology (Hangzhou) Co., Ltd, Hangzhou, China). Further details of the measurements of NMVOCs, $CH_4$, HCHO, trace gases, HONO and photolysis frequencies can be found in the Supporting Information. The meteorological parameters, including wind speed, wind direction, temperature and relative humidity, were obtained from the National Meteorological Information Center (http://data.cma.cn/). The sensors are approximately 3000 meters away from the measurement area.

**2.3 Atmospheric chemical transport model:SOSAA**

SOSAA is a column (or one-dimensional) chemical transport model that was first developed by (Boy et al., 2011). A more detailed description of its newest version can be found in (Zhou et al., 2017a;Zhou et al., 2017b). In this study, a box model version of SOSAA was used, in which the meteorological variables, including air temperature, air pressure, relative humidity and incoming global radiation, were directly read from the measurement data. The chemistry scheme was

generated by MCM v3.3.1 (http://mcm.leeds.ac.uk/MCMv3.3.1) (Jenkin et al., 1997;Jenkin et al., 2015;Saunders et al., 2003) and then converted to Fortran code with kinetic pre-processor (KPP) (Damian et al., 2002). The mixing ratios of chemical species included in the chemistry scheme, e.g., $O_3$, NO, $NO_2$, $SO_2$, CO, HONO, HCHO, isoprene and acetone, were read from the measured data when available. Ten OVOCs (acrolein (ACR), $C_2H_5CHO$, methacrolein (MACR), $C_3H_7CHO$, methylvinylketone (MVK), methylethylketone (MEK), 2-pentanone (MPRK), $C_4H_9CHO$, diethylketone (DIEK), $C_5H_{11}CHO$) were excluded from the input list, despite also being measured, because their simulated concentrations were compared with the measurement data to validate the model performance. Seven photolysis rates (J_$O^1D$, J_HCHO_M, J_$NO_2$, J_$H_2O_2$, J_HONO, J_$NO_3$_M and J_$NO_3$_R) were also read from the measurement data, and the related photochemical reactions are shown below:

$O_3$ -> $O_2$ + O1D: J_$O^1D$ (R1)

HCHO -> $H_2$ + CO: J_HCHO_M (R2)

$NO_2$ -> NO + $O^3P$: J_$NO_2$ (R3)

$H_2O_2$ -> 2 OH: J_$H_2O_2$ (R4)

HONO -> OH + NO: J_HONO (R7)

$NO_3$ -> NO + $O_2$: J_$NO_3$_M (R8)

$NO_3$ -> $NO_2$ + $O^3P$: J_$NO_3$_R. (R9)

The other photolysis rates were calculated using the incoming global radiation. The deposition velocities of all noninput species were set to 0.01 m $s^{-1}$ and the boundary layer height was assumed to be 1 km (Lu et al., 2013;Zhu et al., 2020). The simulated OVOCs were also assumed to condense onto pre-existing aerosols. Their condensation sinks were set to make their simulated concentrations approach the measurement data. The model time step was set to 10 s, and the data were output every half an hour. All the input data were interpolated to the model time step.

**2.4 Speciated oxidant reactivity**

Atmospheric oxidant reactivity is a measure of the strength of the reaction of trace gases with an oxidant (OH, $O_3$ or $NO_3$) (Kovacs et al., 2003;Mogensen et al., 2015). High oxidant reactivity values correspond to short lifetimes and long-lived species have low reactivities. The total OH, $NO_3$ and $O_3$ reactivities can be calculated by Eq. (1)-(3), respectively.

$$\text{The total OH reactivity} = \sum k_{OH+NMVOC_i}[NMVOC_i] + k_{OH+CH_4}[CH_4] + k_{OH+CO}[CO] + k_{OH+NO}[NO] + k_{OH+NO_2}[NO_2] + k_{OH+SO_2}[SO_2] + k_{OH+O_3}[O_3] + \cdots \quad (1)$$

$$\text{The total } NO_3 \text{ reactivity} = \sum k_{NO_3+NMVOC_i}[NMVOC_i] + k_{NO_3+CH_4}[CH_4] + k_{NO_3+NO}[NO] + k_{NO_3+NO_2}[NO_2] + k_{NO_3+SO_2}[SO_2] + \cdots \quad (2)$$

$$\text{The total } O_3 \text{ reactivity} = \sum k_{O_3+NMVOC_i}[NMVOC_i] + k_{O_3+CH_4}[CH_4] + k_{O_3+NO}[NO] + k_{O_3+NO_2}[NO_2] + \cdots \quad (3)$$

In the above equations, the temperature-dependent reaction rate coefficients (in $cm^3$ $molecule^{-1}$ $s^{-1}$) for OH-$NMVOC_i$ ($k_{OH+NMVOC_i}$), OH-CO ($k_{OH+CO}$), $NO_3$-$NMVOC_i$ ($k_{NO_3+NMVOC_i}$) and $O_3$-$NMVOC_i$ ($k_{O_3+NMVOC_i}$) are from (Atkinson and Arey, 2003;Atkinson et al., 2006;Atkinson et al., 1983;Salgado et al., 2008) and MCM v3.3.1 via the website: http://mcm.leeds.ac.uk/MCM (last accessed: 25 March 2020). OH-NO ($k_{OH+NO}$), OH-$NO_2$ ($k_{OH+NO_2}$), OH-$SO_2$ ($k_{OH+SO_2}$), OH-$O_3$ ($k_{OH+O_3}$), $NO_3$-NO ($k_{NO_3+NO}$), $NO_3$-$NO_2$ ($k_{NO_3+NO_2}$), $NO_3$-$SO_2$ ($k_{NO_3+SO_2}$), $O_3$-NO ($k_{O_3+NO}$) and $O_3$-$NO_2$ ($k_{O_3+NO_2}$) are from (Atkinson et al., 2004). The temperature-dependent reaction rate coefficients are listed in Table S1 in the Supplementary Materials. $[NMVOC_i]$, $[CH_4]$, $[CO]$, $[NO]$, $[NO_2]$, $[SO_2]$ and $[O_3]$ are the corresponding number concentrations (in molecules $cm^{-3}$).

**2.5 Atmospheric oxidation capacity (AOC)**

The term "oxidation capacity" of an oxidant $X$ ($NO_3$, OH and $O_3$) is defined as the sum of the respective oxidation rates of the molecules $Y_i$ (NMVOCs, $CH_4$ and CO) (Geyer et al., 2001).

$$\text{AOC} = \sum_{i=1} k_{Y_i-X}[Y_i][X] = \sum_{i=1} R_X^{Y_i}[X] \quad (4)$$

Here, $[Y_i]$ and $[X]$ are number concentrations of molecule $Y_i$ and oxidant $X$, respectively. $k_{Y_i-X}$ is the temperature-dependent reaction rate coefficient of molecule $Y_i$ with oxidant $X$. $R_X^{Y_i}$ is the oxidant $X$ reactivity of molecule $Y_i$.

**3 Results and discussion**

**3.1 Overview of measurements**

For the data evaluation, all measurements were averaged over 1-hour time intervals. The measured concentrations of major pollutants and meteorological parameters at Xianghe are depicted in Figure 2, while the mean diurnal profiles are shown in Figure S1. During the campaign, sunny weather conditions prevailed with temperatures ranging from 25℃ to 31℃ during the daytime. Wind data suggested that the prevailing wind was from the eastern sampling site with a mean wind

speed of 1.0 m $s^{-1}$ ranging from 0.3 m $s^{-1}$ to 1.4 m $s^{-1}$, and the average relative humidity was 85%, reaching up to 96% during the night (Figure 2). Campaign-averaged maximum and minimum $SO_2$ mixing ratios of 3.6 ppb at approximately 14:00 h and 2.3 ppb during the nighttime were obtained (Figure S1a). For $JO^1D$, $JNO_2$ and $JNO_3$, a similar maximum at ~14:00 h was observed, with maximum values of 2.1 $\times 10^{-5}$ $s^{-1}$, 5.3 $\times 10^{-3}$ $s^{-1}$ and 1.3 $\times 10^{-1}$ $s^{-1}$, respectively (Figure S1k-m). The maximum $JO^1D$ at this site was comparable with those in Shanghai and Chongqing but higher than that in Guangzhou and lower than that in Beijing (Tan et al., 2019;Wang et al., 2019). The observed mean daily maxima of $JNO_2$ at this site were higher than those observed in the eastern Mediterranean (Gerasopoulos et al., 2012) but lower than those in Beijing (Wang et al., 2019).

The diurnal maximum $O_3$ concentration was 72 ppb at this site (Figure S1d), which was in line with that observed in Beijing (72 ppb) but higher than those measured in Guangzhou (65 ppb) and Chongqing (56 ppb) and lower than that observed in Shanghai (80 ppb) (Tan et al., 2019). The $O_3$ precursors, CO, $NO_x$, $CH_4$ and NMVOCs, are shown in Figure 2 and Figure S1. The trend of NMVOCs was inversely related to that of $O_3$. When the NMVOCs concentrations in the atmosphere accumulates to a certain level, as photochemical reactions progress, the $O_3$ concentration gradually increases, and the NMVOCs concentrations gradually decreases (Kansal, 2009;Song et al., 2018). CO and $NO_x$ showed a similar diurnal profile with a maximum during rush hour and a minimum in the afternoon (Figure S1b and c), suggesting that both CO and $NO_x$ originated from the same source (enhanced traffic emission), and/or were manipulated by the same factor (e.g., poor dilution conditions). During the campaign, the average mixing ratio of total NMVOC was 32.4 ppb, with the highest contributions from alkanes (13.2 ppb, 40.6%), followed by OVOCs (12.0 ppb, 37.0%), aromatics (4.3 ppb, 13.2%) and alkenes (3.0 ppb, 9.2%). The top 10 NMVOC species (Figure 3a), in terms of emissions, consisted of HCHO (7.0 ppb), propane (3.7 ppb), acetone (3.2 ppb), ethane (3.2 ppb), n-butane (1.9 ppb), m/p-xylene (1.6 ppb), iso-pentane (1.3 ppb), ethylene (1.3 ppb), iso-butane (1.1 ppb) and isoprene (1.0 ppb), accounting for 78.4% of the total NMVOC concentration. As typical tracers of vehicle-related emissions, propane, ethane, ethene, butanes and pentanes were present in high concentrations, suggesting that vehicle-related emissions were likely to be the dominant source of NMVOCs at this site. In addition, the shape of the diurnal variations in total NMVOCs backed the presence of vehicle-related emissions, presenting higher mixing ratios during

the early morning and from evening to midnight, which may be related to enhanced traffic emissions during rush hours and poor dilution conditions (Yuan et al., 2009;He et al., 2019;Tan et al., 2019). On the other hand, the mixing ratios of total NMVOCs began to decrease at 10:00 h and maintained a broad trough during daytime hours, probably due to increased photochemical removal processes favoring the destruction of NMVOCs, the elevated planetary boundary layer (PBL) promoting the dispersion of NMVOCs and/or reduced NMVOC emissions reducing the levels of NMVOCs (He et al., 2019;Zheng et al., 2018). In contrast, the OVOC concentrations (Figure S1i) increased from a minimum near sunrise and reached a maximum in the late afternoon, reflecting the accumulation of OVOCs during the photochemically active period of the day and illustrating the time profile of the formation of secondary species (Yuan et al., 2012).

### 3.2 Reactivities of OH, $NO_3$ and $O_3$

#### 3.2.1 OH reactivity

The OH reactivity of trace gases was categorized into $SO_2$, CO, $O_3$, $NO_x$, $CH_4$ and total NMVOCs, which were grouped into alkanes, alkenes, aromatics and OVOCs (Table S1 lists the NMVOCs included in each group), as shown in Figure 4a and 4b. The total OH reactivity was between 9.2 and 69.6 $s^{-1}$, with an average of 27.5±9.7 $s^{-1}$ (± standard deviation). Statistically, the average total OH reactivity was much higher than those determined in Beijing (16.4 $s^{-1}$ and 20±11 $s^{-1}$) (Tan et al., 2019;Yang et al., 2017), Shanghai (13.5 $s^{-1}$) (Tan et al., 2019), Chongqing (17.8 $s^{-1}$) (Tan et al., 2019), Jinan (19.4±2.1 $s^{-1}$) (Lyu et al., 2019), Wangdu (10-20 $s^{-1}$) (Fuchs et al., 2017), Houston (9-22 $s^{-1}$) (Mao et al., 2010), London (18.1 $s^{-1}$) (Whalley et al., 2016) and Nashville (11.3 ± 4.8 $s^{-1}$) (Kovacs et al., 2003), but was comparable to or lower than those in Heshan (31±20 $s^{-1}$) (Yang et al., 2017), Backgarden (mean maximum value of 50 $s^{-1}$) (Lou et al., 2010) and New York (25 $s^{-1}$) (Ren et al., 2006b). The OH reactivity towards $SO_2$, CO and NOx was higher than the values reported in various Chinese cities (Xu et al., 2011;Zhu et al., 2020;Liu et al., 2009) (Table 1). It should be noted that the OH reactivity in this study was calculated from the sum of the products of measured species and their rate coefficients for reactions with OH, and does not involve species that were not measured, such as monoterpenes and alcohols. Previous studies have shown that there are some discrepancies between the actual measured values and the calculated values of OH reactivity, which may be attributed to missing OH reactivity that originates from VOC oxidation products of

both biogenic and anthropogenic origin (Di Carlo et al., 2004;Dolgorouky et al., 2012;Yoshino et al., 2006;Zhu et al., 2020). Therefore, the OH reactivity calculated in this study is somewhat underestimated.

The total OH reactivity was mainly contributed by $NO_x$ (12.0±7.1 $s^{-1}$, 43.7%), followed by NMVOCs (7.9±4.8 $s^{-1}$, 28.5%), CO (7.2±2.6 $s^{-1}$, 26.0%) and $CH_4$ (0.3±0.1 $s^{-1}$, 1.3%) and to a lesser extent by $SO_2$ and $O_3$ (0.2±0.1 $s^{-1}$, 0.6%), indicating the strong influence of anthropogenic emissions in Xianghe. The majority of total OH reactivity values were below 30 $s^{-1}$, as seen in the frequency distribution, which was dominated by the sum of low-OH-reactivity contributions and less influenced by single compounds with high OH reactivity (Figure S2a-f). Specifically, the cumulative frequency distribution (Figure S3a) clearly showed that the OH reactivity at values >40 $s^{-1}$ was dominated entirely by OH reactivity towards NOx, and the OH reactivity at values from 20-40 $s^{-1}$ was nearly completely dominated by OH reactivity towards NOx and total NMVOCs. In general, the frequency distributions and cumulative frequency distributions of OH reactivity highlighted the necessity of considering a large number of species to obtain a better understanding of OH reactivity.

The OH reactivity towards total NMVOCs was 7.9±4.8 $s^{-1}$, which was much lower than those in Beijing (11.2 $s^{-1}$) and Heshan (18.3 $s^{-1}$) (Yang et al., 2017) due to the higher content of reactive hydrocarbons (e.g., alkenes and aromatics) in Beijing and Heshan and due to the unmeasured species (e.g., acetaldehyde) in this study. Alkenes (3.4±3.7 $s^{-1}$, 42.9%) dominated over OVOCs (2.4±1.5 $s^{-1}$, 30.2%), aromatics (1.5±1.7 $s^{-1}$, 18.6%) and alkanes (0.7±0.5 $s^{-1}$, 8.3%) in the OH reactivity towards total NMVOCs. The majority of the values of OH reactivity towards total NMVOCs were below 13 $s^{-1}$ (Figure S4a-d). The cumulative frequency distribution showed that the OH reactivity towards total NMVOCs at values of > 6 $s^{-1}$ was dominated by OH reactivity towards alkenes, aromatics and OVOCs, and that the OH reactivity towards total NMVOCs at values of <6 $s^{-1}$ was dominated by OH reactivity towards alkanes (Figure S5). Alkanes accounted for >50% of the mixing ratio of NMVOCs, but only 8.3% of the OH reactivity towards total NMVOCs. In contrast, aromatics, alkenes and OVOCs accounted for 44.6% of the mixing ratio of NMVOCs, providing 91.7% of the OH reactivity towards total NMVOCs. Significantly, isoprene accounted for only 4% of the mixing ratio of NMVOCs but provided 31.2% of the OH reactivity towards total NMVOCs.

This result was explained by (1) the relatively low concentration of aromatics, alkenes and OVOCs measured during the campaign, (2) the relatively high concentration of isoprene and (3) the generally large isoprene reaction rate coefficient with OH ($101\times10^{-12}$ $cm^3$ $molecule^{-1}$ $s^{-1}$) (Atkinson et al., 2006). The top 10 species, in terms of OH reactivity towards total NMVOCs, consisted of isoprene, HCHO, m/p-xylene, ethylene, hexanal, o-xylene, propylene, styrene, MACR and cis-2-butene (Figure 3b). These species contributed only 39.1% to NMVOC emissions but accounted for 80.3% of OH reactivity towards total NMVOCs. As shown in Table 1, the OH reactivity towards the speciated NMVOCs in this study was basically within the values reported in various Chinese cities (Tan et al., 2019;Xu et al., 2011;Yang et al., 2017;Zhu et al., 2020).

The mean diurnal profiles of the OH reactivity of trace gases and NMVOCs are presented in Figure 5a-f and Figure 6a-d, respectively. In general, the total OH reactivity was the lowest in the afternoon and the highest during rush hours, reaching a maximum of 33.0 $s^{-1}$ during the morning rush hour and a night-time peak of 30.5 $s^{-1}$ (Figure 5a). Most campaigns have also reported slightly higher OH reactivity in the morning traffic rush hour, which can be explained by higher levels of reactive gases such as NO and NMVOCs due to heavy traffic, as well as slower reactions (Fuchs et al., 2017;Yang et al., 2016). A similar diurnal profile was also observed for contributions from $NO_x$, CO, alkane and aromatic species, which are typically connected to emissions from anthropogenic activities. The shape of the total OH reactivity diurnal pattern was slightly shifted in the dorection of OH reactivity towards NOx, strengthening the idea that the local pollution in Xianghe was possibly impacted by traffic emissions. However, a different diurnal behavior to that of the above species was observed for alkenes (Figure 6b) and OVOCs (Figure 6d), which are emitted by plants or produced photochemically. The OH reactivity from OVOCs increased by a factor of approximately 2 from nighttime to daytime, suggesting that during the daytime, dilution or chemical removal had a weaker influence on the observed OVOCs than fresh production by photochemistry. The opposite diurnal variation was reported in Wangdu, which showed a weak diurnal variation with a decrease by a factor of approximately 2 from the morning to the evening (Fuchs et al., 2017). The diurnal profile of OH reactivity towards isoprene appears to be the major driver for the diurnal profile of OH reactivity towards alkenes. Biogenic isoprene is dependent on temperature and light intensity (Chang et al., 2014), and anthropogenic isoprene is predominantly emitted by road traffic

(Ye et al., 1997); hence, the OH reactivity from alkenes increased during the daytime, with a morning peak of 4.1 $s^{-1}$ at 9:00 h and a night-time peak of 7.4 $s^{-1}$ at 18:00 h. Many rainforest campaigns have also reported a significant diurnal pattern with higher OH reactivity from alkenes and OVOCs at noontime or a maximum at the beginning of the night (Yang et al., 2016). Notably, the large amplitude of the standard deviation bars highlighted the large diel variability.

**3.2.2 $NO_3$ reactivity**

The $NO_3$ reactivity of trace gases was categorized into $SO_2$, $NO_x$, $CH_4$ and NMVOCs, as shown in Figure 4c and d. The campaign-averaged values of total $NO_3$ reactivity were 2.2±2.6 $s^{-1}$, ranging from 0.7 $s^{-1}$ to 27.5 $s^{-1}$. The average total $NO_3$ reactivity was much higher than those determined during the IBAIRN campaign (Liebmann et al., 2018a) and at a rural mountain site (988 m a.s.l.) in southern Germany in 2017 (Liebmann et al., 2018b) due to higher contributions from $NO_x$. We noted that $NO_x$ was by far the main contributor to the total $NO_3$ reactivity, representing 99% of the total $NO_3$ reactivity on average. NO exhibited the most prominent contribution to the total $NO_3$ reactivity and represented an average of 78.0% of the total $NO_3$ reactivity. In contrast to NO, $NO_2$ had a maximum contribution during the night-time and represented, on average, 27% of the total $NO_3$ reactivity. The $NO_3$ reactivity towards $CH_4$, NMVOCs and $SO_2$ was very minor, accunting for no more than 1% of the total $NO_3$ reactivity over the whole campaign. The majority of the total $NO_3$ reactivity values were below 3 $s^{-1}$, but values below 5.5 $\times 10^{-5}$ $s^{-1}$, 0.1 $s^{-1}$, 3 $s^{-1}$ and $1\times 10^{-8}$ $s^{-1}$ were observed for $NO_3$ reactivity towards $CH_4$, total NMVOCs, NOx and $SO_2$, respectively, as seen in the frequency distribution (Figure S2g-k). The cumulative frequency distribution clearly showed that the total $NO_3$ reactivity at low and high values was entirely dominated by $NO_3$ reactivity towards $SO_2$ and NOx, respectively (Figure S3b). In total, the frequency distributions and cumulative frequency distributions of $NO_3$ reactivity highlighted the necessity of considering a large number of species to obtain a complete picture of $NO_3$ reactivity.

The $NO_3$ reactivity towards total NMVOCs was $2.4\pm3.0\times10^{-2}$ $s^{-1}$ on average with a minimum of $1.1\times10^{-3}$ $s^{-1}$ and a maximum of 0.3 $s^{-1}$. The largest fraction of attributed $NO_3$ reactivity towards total NMVOCs was provided by alkenes (77.8%), followed by aromatics (20.7%) and OVOCs (1.3%). The measured alkanes played virtually no role in $NO_3$ reactivity towards total NMVOCs, although they accounted for more than 50% of the mixing ratio of NMVOCs. This result can be

largely explained by the fact that the reaction rate coefficients of alkenes, aromatics and OVOCs with $NO_3$ are 1-5 orders of magnitude higher than the alkane reaction rate coefficients with $NO_3$ (Atkinson and Arey, 2003;Atkinson et al., 2006). The majority of the $NO_3$ reactivity values towards alkanes, alkenes, aromatics and OVOCs were below $5.0\times10^{-5}$ $s^{-1}$, 0.1 $s^{-1}$, $1.0\times10^{-2}$ $s^{-1}$ and $1.0\times10^{-3}$ $s^{-1}$, respectively (Figure S4e-f). The cumulative frequency distribution showed that the $NO_3$ reactivity towards total NMVOCs at values of > 0.1 $s^{-1}$ was entirely dominated by $NO_3$ reactivity towards alkenes, the $NO_3$ reactivity towards total NMVOCs at values from 0.01-0.1 $s^{-1}$ was dominated by $NO_3$ reactivity towards alkenes and aromatics, and the $NO_3$ reactivity towards total NMVOCs at values of $<1.0\times10^{-5}$ $s^{-1}$ was entirely dominated by $NO_3$ reactivity towards alkanes (Figure S6). The top ten species in terms of $NO_3$ reactivity towards total NMVOCs consisted of isoprene, styrene, cis-2-butene, trans-2-butene, cis-2-pentene, hexanal, HCHO, propylene, 1,3-butadiene and trans-2-pentene (Figure 3c). These species contributed only 27.7% to NMVOC emissions but accounted for 99.2% of the $NO_3$ reactivity towards total NMVOCs.

Total $NO_3$ reactivity displayed a weak diel variation with a campaign-averaged morning peak value of 4.0 $s^{-1}$ at 6:00-7:00 h (Figure 5g). The diurnal profile of $NO_3$ reactivity towards NOx (Figure 5i) appears to be the major driver for the diurnal profile of total $NO_3$ reactivity. The morning peak value of total $NO_3$ reactivity could be explained by the accumulation of $NO_x$ due to traffic emissions that are released into the shallow nocturnal boundary layer during the morning rush hours. In contrast, the average diurnal profile of $NO_3$ reactivity towards total NMVOCs (Figure 5k) had a maximum at 18:00 h, which was slightly shifted in the direction of $NO_3$ reactivity towards alkenes (Figure 6j). The evening peak value of $NO_3$ reactivity towards total NMVOCs could be accounted for by the accumulation of alkenes due to vegetation emissions and traffic emissions that are released into the shallow nocturnal boundary layer. $NO_3$ reactivity towards alkanes (Figure 6e), alkenes (Figure 6f), aromatics (Figure 6g), OVOCs (Figure 6h) and $SO_2$ (Figure 5h) played virtually no role in the diurnal variations in total $NO_3$ reactivity and $NO_3$ reactivity towards total NMVOCs but exhibited a more distinct diurnal profile.

**3.2.3 $O_3$ reactivity**

The $O_3$ reactivity of trace gases was categorized into $NO_x$, $CH_4$ and total NMVOCs, as shown in Figure 4e and f. The total $O_3$ reactivity at the site varied between a minimum of $3.3\times10^{-4}$ $s^{-1}$ and

a maximum of $1.8\times10^{-2}$ $s^{-1}$ and was $1.2\pm1.7\times10^{-3}$ $s^{-1}$ on average. NO exhibited the most prominent contribution to the total $O_3$ reactivity and represented >99% of the total $O_3$ reactivity on average, whereas nearly all other contributions were < 1%. This result can be largely accounted for by the generally large NO reaction rate coefficients with $O_3$ ($1.8\times10^{-14}$ $cm^3$ $molecule^{-1}$ $s^{-1}$) (Atkinson et al., 2006), which are several orders of magnitude higher than the reaction rate coefficients of $NO_2$, alkanes, alkenes, aromatics and OVOCs with $NO_3$ (Atkinson et al., 2006;Atkinson and Arey, 2003;Yuan et al., 2013;Ferracci et al., 2018;Jenkin et al., 2015). The majority of the total $O_3$ reactivity values were below $2\times10^{-3}$ $s^{-1}$, but values below $5.5\times10^{-10}$ $s^{-1}$, $2\times10^{-6}$ $s^{-1}$ and $2\times10^{-3}$ $s^{-1}$ were observed for the $O_3$ reactivity towards $CH_4$, total NMVOCs and NOx, respectively, as seen in the frequency distribution (Figure S2l-o). The cumulative frequency distribution clearly showed that the total $O_3$ reactivity at low and high values was entirely dominated by $O_3$ reactivity towards $CH_4$ and NOx, respectively (Figure S3c). Generally, the frequency distributions and cumulative frequency distributions of $O_3$ reactivity highlight the necessity of considering a large number of species to obtain a complete picture of $O_3$ reactivity.

The $O_3$ reactivity towards total NMVOCs was $1.1\pm0.8\times10^{-6}$ $s^{-1}$ on average, ranging from a minimum of $2.5\times10^{-7}$ $s^{-1}$ to a maximum of $1.0\times10^{-5}$ $s^{-1}$. Alkenes clearly dominated the $O_3$ reactivity towards total NMVOCs, with a campaign-averaged contribution of 94.0%. Aromatics were the second largest contributor, comprising an average of 5.2% of the $O_3$ reactivity towards total NMVOCs. In comparison, OVOCs accounted for only 0.8% of the $O_3$ reactivity towards total NMVOCs. In contrast, the measured alkanes played nearly no role in the $O_3$ reactivity towards total NMVOCs due to their small reaction rate coefficients with $O_3$ (<$1.0\times10^{-23}$ $cm^3$ $molecule^{-1}$ $s^{-1}$) (Atkinson and Arey, 2003;Atkinson et al., 2006). The majority of the $O_3$ reactivityvalues towards alkanes, alkenes, aromatics and OVOCs were below $5.0\times10^{-12}$ $s^{-1}$, $3.0\times10^{-6}$ $s^{-1}$, $2.0\times10^{-7}$ $s^{-1}$ and $2.0\times10^{-8}$ $s^{-1}$, respectively (Figure S4i-l). The cumulative frequency distribution (Figure S7) clearly showed that the $O_3$ reactivity towards total NMVOCs at >$1.0\times10^{-7}$ $s^{-1}$ was dominated by $O_3$ reactivity towards alkenes and aromatics, the $O_3$ reactivity towards total NMVOCs between $1.0\times10^{-9}$ $s^{-1}$ and $1.0\times10^{-7}$ $s^{-1}$ was dominated by $O_3$ reactivity towards alkenes, aromatics and OVOCs, and the $O_3$ reactivity towards NMVOCs <$1.0\times10^{-11}$ $s^{-1}$ was entirely dominated by $O_3$ reactivity towards alkanes. In terms of individual species, isoprene, cis-2-butene, trans-2-butene, cis-2-pentene,

436 propylene, styrene, ethylene, 1-butene, trans-2-pentene and 1-pentene were the top ten species
437 (Figure 3d), accounting for 28%, 25%, 20%, 8%, 7%, 5%, 5%, 3%, 2% and 1%, respectively, of the
438 $O_3$ reactivity towards total NMVOCs and 3.1%, 0.3%, 0.1%, 0.1%%, 1%, 0.4%, 4.1%, 0.4% 0.1%
439 and 0.1%, respectively, of the total NMVOC emissions.

440 Compared with the OH and $NO_3$ reactivities, $O_3$ reactivity displayed a much weaker diel
441 variation, especially the $O_3$ reactivity towards alkenes and aromatics, as shown in Figure 5 and
442 Figure 6. This weakness can be explained by the following reasons. First, for a given species, the
443 reaction rate coefficients with $O_3$ were much smaller than the corresponding reaction rate
444 coefficients with OH and $NO_3$. For example, the ethylene reaction rate coefficients with OH
445 ($8.52\times10^{-12}$ $cm^3$ $molecule^{-1}$ $s^{-1}$) and $NO_3$ ($2.05\times10^{-16}$ $cm^3$ $molecule^{-1}$ $s^{-1}$) are 6 and 2 orders of
446 magnitude higher, respectively, than the ethylene reaction rate coefficient with $O_3$ ($1.59\times10^{-18}$ $cm^3$
447 $molecule^{-1}$ $s^{-1}$) (Atkinson and Arey, 2003;Atkinson et al., 2006). Second, the high-emission species
448 reaction rate coefficients with $O_3$ are smaller than the low-emission species reaction rate coefficients
449 with $O_3$. For instance, the m/p-xylene (one of the top five species in terms of emissions) reaction
450 rate coefficient with $O_3$ ($<1.0\times10^{-20}$ $cm^3$ $molecule^{-1}$ $s^{-1}$) are much smaller than the 1-hexene (one of
451 the bottom five emissions species) reaction rate coefficients with $O_3$ ($1.13\times10^{-17}$ $cm^3$ $molecule^{-1}$ $s^{-1}$)
452 (Atkinson and Arey, 2003;Atkinson et al., 2006). The above two factors largely weaken the diurnal
453 variation in $O_3$ reactivity.

454 **3.3 Implications for OH, $NO_3$ and $O_3$ reactivity-based NMVOC control strategies**

455 Table 2 lists the top 10 NMVOC species (excluding isoprene) in terms of concentration, OH,
456 $NO_3$ and $O_3$ reactivities, and their corresponding contributions to concentrations, and OH, $NO_3$ and
457 $O_3$ reactivities. The order of the major OH, $NO_3$ and $O_3$ reactivity-contributing species differed
458 significantly from that of concentration-contributing species. Therefore, NMVOC control strategies
459 based on OH, $NO_3$ and $O_3$ reactivities differ significantly from those based on concentrations.

460 From the perspective of concentration, HCHO, propane, acetone, ethane, n-butane, m/p-xylene,
461 iso-pentane, ethylene, iso-butane and n-pentane should be targeted. If these 10 species were fully
462 controlled, it would lead to an NMVOC concentration reduction of 79.9% with OH, $NO_3$ and $O_3$
463 reactivity reductions of only 58.4%, 2.1% and 6.4%, respectively. These species are mainly from
464 fuel combustion and vehicle exhaust (Song et al., 2018;Liu et al., 2017); hence, from the perspective

of the current emission-based limits, we recommend that the priorities for the control of NMVOC sources include fuel combustion and vehicle exhaust.

From the perspective of OH reactivity, HCHO, m/p-xylene, ethylene, hexanal, o-xylene, propylene, styrene, MACR, cis-butene and MVK were the key species. If the releases of these compounds were reduced to zero without any offset, OH reactivity would be reduced by 73.3% with an NMVOC concentration reduction of 38.1%, a $NO_3$ reactivity reduction of 86.4% and $O_3$ reactivity reduction of 55.7%. From the perspective of $NO_3$ reactivity, the top 10 NMVOC species consisted of styrene, cis-2-butene, trans-2-butene, cis-2-pentene, hexanal, HCHO, propylene, 1,3-butadiene, trans-2-pentene and 1-butene. If the concentrations of these species were completely eliminated, it would reduce $NO_3$ reactivity by 97.8% with an NMVOC concentration reduction of 25.8%, an OH reactivity reduction of 49.7% and an $O_3$ reactivity reduction of 91.8%. From the perspective of $O_3$ reactivity, cis-2-butene, trans-2-butene, cis-2-pentene, propylene, styrene, ethylene, 1-butene, trans-2-pentene, 1-pentene and MACR should be the key targets for control. If the concentrations of these compounds were reduced to zero without any offset, it would lead to an $O_3$ reactivity reduction of 98.9% with an NMVOC concentration reduction of 7.3%, an OH reactivity reduction of 22.3% and a $NO_3$ reactivity reduction of 94.2%. The top ten species associated with OH, $NO_3$ and $O_3$ reactivities are mainly from traffic-related emissions, industry and solvent usage (Song et al., 2018;Liu et al., 2017;Chen et al., 2014). Therefore, in terms of reactivity-based limits, we recommend that the priorities for the control of NMVOC sources include traffic-related emissions, industry and solvent usage.

Clearly, species with large concentrations do not necessarily have high OH, $NO_3$ and $O_3$ reactivities, and a small concentration reduction can result in a maximum reduction in reactivity. The key NMVOC species in terms of OH, $NO_3$ and $O_3$ reactivities also differed from each other. However, reducing the concentrations of propylene, styrene and cis-2-butene may likely achieve a win-win-win situation. Although the above comparisons were made under the assumption that concentrations would be significantly reduced, it is obvious that OH, $NO_3$ and $O_3$ reactivity-based control strategies are more efficient than concentration-based policies in terms of reducing NMVOC pollution. Overall, the combined integration and comparison of OH, $NO_3$ and $O_3$ reactivities towards NMVOCs could provide useful suggestions for VOC pollution control in the North China Plain.

494 **3.4 AOC**

495 **3.4.1 Modeling OVOCs, OH, $HO_2$, $RO_2$ and $NO_3$ by SOSAA**

496 With the appropriate setup of the condensation sinks for the ten calculated OVOCs (ACR,
497 $C_2H_5CHO$, MACR, $C_3H_7CHO$, MVK, MEK, MPRK, $C_4H_9CHO$, DIEK and $C_5H_{11}CHO$), the
498 modeled diurnal mean pattern generally followed the measured pattern within 1 standard deviation
499 of the measurement data, although the model underestimated measurements, predicting values of
500 less than 1 ppb from 19:00 to 24:00h (Figure S8a). With the inclusion of input MTBE and
501 $CH_3COCH_3$ (acetone) which constituted more than 50% of the total OVOCs, the modeled total
502 OVOC concentration agreed better with the measurements than expected (Figure S8b). The modeled
503 diurnal median number concentrations of OH, $HO_2$ and $RO_2$ showed an apparent diurnal pattern
504 with peaks during midday and values approaching zero during night, which resulted from the
505 dependence of their chemical production reactions on incoming solar radiation (Figure S9a, b and
506 c). The midday time (12:00-16:00 h) median number concentrations of OH, $HO_2$ and $RO_2$ were
507 $1.2\times10^7$, $5.9\times10^8$ and $3.7\times10^8$ molecules $cm^{-3}$, respectively, which were comparable to previous
508 studies (Tan et al., 2017). The diurnal variation of in the hourly median $NO_3$ concentration showed
509 two peaks which were consistent with the high chemical production from $NO_2 + O_3$ (Figure S9d).
510 Figure S10 shows the relationship between the modeled OH number concentration and the measured
511 $J\_O^1D$. The coefficient of determination ($R^2$) was 0.86, and the linear regression fit showed that the
512 slope was $6.1\times10^{11}$ $cm^{-3}$ $s^{-1}$ and the intercept was $0.9\times10^6$ $cm^{-3}$. These values were comparable to
513 Tan et al. (2017), except the slope here was approximately 36% higher than the observed fit in Tan
514 et al. (2017).

515 **3.4.2 Overall characteristics of AOC**

516 The loss rates of NMVOCs, $CH_4$ and CO via reactions with OH, $O_3$ and $NO_3$ were calculated.
517 The calculated AOC was up to $4.5\times10^8$ molecules $cm^{-3}$ $s^{-1}$ with a campaign-averaged value of
518 $7.8\times10^7$ molecules $cm^{-3}$ $s^{-1}$, daytime average (06:00-18:00 h) of $1.4\times10^8$ molecules $cm^{-3}$ $s^{-1}$ and
519 nighttime average of $6.7\times10^6$ molecules $cm^{-3}$ $s^{-1}$. As such, the total number of NMVOCs, $CH_4$ and
520 CO molecules depleted during the daytime and nighttime were $6.0\times10^{12}$ and $2.9\times10^{11}$, respectively,
521 per $cm^{-3}$ of air. These AOC levels were higher than those determined at the Tung Chung air quality
522 monitoring station (Xue et al., 2016), a polluted area in Santiago, Chile (Elshorbany et al., 2009)

and the Hong Kong Polytechnic University's air monitoring station at Hok Tsui (Li et al., 2018).

Comparisons of the AOC values calculated from OH, $O_3$ and $NO_3$ and the corresponding oxidation concentrations are shown in Figure 7. The OH and $NO_3$ radical concentrations were simulated by the SOSAA box model. The AOC calculated from OH, $O_3$ and $NO_3$ correlated well with the corresponding oxidation concentrations, with correlation coefficients (r) of 0.91, 0.83 and 0.57, respectively, suggesting that the parameterized AOC here was consistent with that obtained using radical concentration to indicate AOC. Specifically, the average oxidation capacities of OH, $O_3$ and $NO_3$ radicals throughout the entire campaign were $7.7\times10^7$, $1.2\times10^6$ and $1.8\times10^5$ molecules $cm^{-3}$ $s^{-1}$, representing 98.2%, 1.5% and 0.3% of the total oxidation capacity, respectively. The total number of depleted molecules per day due to oxidation by OH, $O_3$ and $NO_3$ was $6.6\times10^{12}$, $1.0\times10^{11}$ and $1.5\times10^{10}$ molecules $cm^{-3}$, respectively; these values were slightly higher than those assessed in a polluted area in Santiago, Chile (Elshorbany et al., 2009). Accordingly, OH radicals are the driving force of AOC in Xianghe, especially during the daytime. Figure 8 shows a comparison of the oxidation capacities of OH, $O_3$ and $NO_3$. On average, the relative contribution of $O_3$ and $NO_3$ oxidation capacities when integrated over 24 hours was less than 4% (Figure 8a-c). OH is the only oxidant of CO in the troposphere. As expected, OH was responsible for 99% of the oxidation capacity regarding NMVOCs, $CH_4$ and CO during the daytime (Figure 8d). The relative contribution of OH to oxidation capacity decreased to 98% when restricting the calculation to NMVOC families alone (Figure 8e). Focusing on the oxidation of unsaturated NMVOCs, OH was the dominant oxidant with a relative proportion of approximately 97% (Figure 8f). Note that the influence of $NO_3$ and $O_3$ on the oxidation of CO and VOCs can be neglected during the daytime. However, elevated relative contributions of $O_3$ and $NO_3$ to oxidation capacity can be observed during the nighttime. As expected, $O_3$ and $NO_3$ accounted for 10% and 2%, respectively, of the oxidation capacity with respect to NMVOCs, $CH_4$ and CO (Figure 9g), but 19% and 3% of NMVOC families alone (Figure 8h) occurred at night. Focusing on the oxidation of unsaturated NMVOCs, $O_3$ and $NO_3$ accounted for 20% and 4%, respectively, of the oxidation capacity (Figure 8i). This quantitative intercomparison of the oxidation capacities of OH, $O_3$ and $NO_3$ confirms the important role of OH in the degradation of NMVOCs, $CH_4$ and CO. Compared with OH and $O_3$, $NO_3$ had a lower contribution during both the daytime and nighttime, which was mainly caused by high NO

552 concentrations (Liebmann et al., 2018b).

553 **4. Summary and conclusions**

554 In the summer of 2018, a comprehensive field campaign was conducted at a suburban site in
555 the North China Plain. Based on simultaneous measurements of $O_3$, CO, $SO_2$, NO, $NO_2$, $JO^1D$,
556 $JNO_2$, $JNO_3$, HONO, HCHO, $CH_4$ and 65 NMVOCs, the reactivities (OH, $NO_3$ and $O_3$ reactivities)
557 towards trace gases and AOC were comprehensively analyzed. The main findings are summarized
558 as follows.

559 The total OH reactivity was between 9.2 and 69.6 $s^{-1}$ with an average of 27.5±9.7 $s^{-1}$, which
560 was mainly contributed by $NO_x$ (43.7%), followed by NMVOCs (28.5%), CO (26.0%) and $CH_4$
561 (1.3%) and $SO_2$ and $O_3$ (0.5%). OH reactivity towards total NMVOCs was 7.9±4.8 $s^{-1}$ and
562 dominated by alkenes (42.9%). The campaign-averaged value of total $NO_3$ reactivity was 2.2±2.6
563 $s^{-1}$, ranging from 0.7 $s^{-1}$ to 27.5 $s^{-1}$. $NO_x$ was the main contributor to the total $NO_3$ reactivity,
564 representing 99% of the total $NO_3$ reactivity on average. $NO_3$ reactivity towards total NMVOCs was
565 $2.4\pm3.0\times10^{-2}$ $s^{-1}$, on average, and it was dominated by alkenes (77.8%). The total $O_3$ reactivity
566 varied between a minimum of $3.3\times10^{-4}$ $s^{-1}$ and a maximum of $1.8\times10^{-2}$ $s^{-1}$ with an average of
567 $1.2\pm1.7\times10^{-3}$ $s^{-1}$. NO exhibited the most prominent contribution to the total $O_3$ reactivity and
568 represented an average of >99% of the total $O_3$ reactivity. The $O_3$ reactivity towards total NMVOCs
569 was $1.1\pm0.8\times10^{-6}$ $s^{-1}$ on average, ranging from $2.5\times10^{-7}$ $s^{-1}$ to $1.0\times10^{-5}$ $s^{-1}$ and dominated by alkenes
570 (94.0%). The total OH, $NO_3$ and $O_3$ reactivities displayed a similar diel variation with the lowest
571 value in the afternoon and the highest value during rush hours, and the diurnal profile of $NO_x$ appears
572 to be the major driver for the diurnal profiles of total OH, $NO_3$ and $O_3$ reactivities. Compared with
573 the OH and $NO_3$ reactivities, $O_3$ reactivity displayed a much weaker diel variation, especially the
574 $O_3$ reactivity towards alkenes and aromatics due to 1) the rate coefficients with $O_3$ being much
575 smaller than the corresponding reaction rate coefficients with OH and $NO_3$ for the same species and
576 2) the high-emission species reaction rate coefficients with $O_3$ being smaller than the low-emission
577 species reaction rate coefficients with $O_3$.

578 The relative OH reactivity towards $NO_x$ and VOCs and the scatter plots of CO-$NO_y$ color-
579 coded with $O_3$ concentrations indicated a VOC-limited regime of $O_3$ formation in Xianghe,
580 suggesting that control of VOCs would be most effective for controlling $O_3$ in Xianghe. OH, $NO_3$

and $O_3$ reactivity-based control strategies are more efficient than concentration-based policies in terms of reducing NMVOC pollution. We suggest that policy makers shift the current concentration -based limits to reactivity-based policies.

The loss rates of NMVOCs, $CH_4$ and CO via reactions with OH, $O_3$ and $NO_3$ were calculated; these loss rates were up to $4.5\times10^8$ molecules $cm^{-3}$ $s^{-1}$ with a campaign-averaged value of $7.8\times10^7$ molecules $cm^{-3}$ $s^{-1}$, daytime average (06:00-18:00 h) of $1.4\times10^8$ molecules $cm^{-3}$ $s^{-1}$ and nighttime average of $6.7\times10^6$ molecules $cm^{-3}$ $s^{-1}$. AOC was dominated by OH radicals ($7.7\times10^7$ molecules $cm^{-3}$ $s^{-1}$, 98.2%), $O_3$ ($1.2\times10^6$ molecules $cm^{-3}$ $s^{-1}$, 1.5%) and $NO_3$ radicals ($1.8\times10^5$ molecule $cm^{-3}$ $s^{-1}$, 0.3%), suggesting that the OH radical is the driving force of the oxidation capacity in the atmosphere in Xianghe, especially during the daytime. The reaction with OH radical was the dominant contributor to the loss rate for NMVOCs except for trans-2-butene, cis-2-butene and trans-2-pentene, where the reaction with $O_3$ was more important for their loss rates during the nighttime. Oxidation by $NO_3$ radicals was more important than oxidation by anthropogenic hydrocarbons for the nighttime averaged loss rate of isoprene.

Our study provides useful insights for VOC pollution control in a typical suburban site in the North China Plain. Further studies, especially direct observations of OH and $NO_3$ radicals, OH and $NO_3$ reactivity measurements and speciated measurements, are required to further explore trace gas reactivity and AOC.

**Acknowledgement**

This study was financially supported by the Ministry of Science and Technology of China (2017YFC0210000), Beijing Major Science and Technology Project (Z181100005418014). All referenced supplemental figures and tables can be found in the supporting information. The authors are grateful to all staff and workers from the Xianghe Atmospheric Observatory of Institute of Atmospheric Physics (IAP) of the Chinese Academy of Sciences for their support during the sampling campaign. We also acknowledge National Meteorological Information Center for providing high quality meteorology parameters. Putian Zhou would also like to acknowledge the University of Helsinki Three Year Grant ("AGES": 2018-2020).

**Competing financial interests**

The authors declare no competing financial interests.

## Author contributions

Y.W designed the research. Y.Y and D.Y, S.Z, D.J, Y.W conducted the measurements. Y.Y and Y.W interpreted the data and write the paper. P.Z and D.C conducted SOSAA simulation. All the authors contributed to discussing results and commenting on the paper.

## Reference


Asaf, D., Pedersen, D., Matveev, V., Peleg, M., Kern, C., Zingler, J., Platt, U., and Luria, M.: Long-Term Measurements of $NO_3$ Radical at a Semiarid Urban Site: 1. Extreme Concentration Events and Their Oxidation Capacity, Environ Sci Technol, 43, 9117-9123, doi:10.1021/es900798b, 2009.

Atkinson, R., Aschmann, S. M., and Jr., J. N. P.: Kinetics of the gas-phase reactions of OH radicals with a series of α,β-unsaturated carbonyls at 299 ± 2 K, International Journal of Chemical Kinetics, 15, 75-81, doi:10.1002/kin.550150108, 1983.

Atkinson, R., and Arey, J.: Atmospheric Degradation of Volatile Organic Compounds., Chemical Reviews, 103, 4605-4638, doi:10.102/cr0206420, 2003.

Atkinson, R., Baulch, D. L., Cox, R. A., Crowley, J. N., Hampson, R. F., Hynes, R. G., Jenkin, M. E., Rossi, M. J., and Troe, J.: Evaluated kinetic and photochemical data for atmospheric chemistry: Volume I - gas phase reactions of Ox, HOx, NOx and SOx species, Atmos. Chem. Phys., 4, 1461-1738, doi:10.5194/acp-4-1461-2004, 2004.

Atkinson, R., Baulch, D. L., Cox, R. A., Crowley, J. N., Hampson, R. F., Hynes, R. G., Jenkin, M. E., Rossi, M. J., Troe, J., and IUPAC Subcommittee: Evaluated kinetic and photochemical data for atmospheric chemistry : Volume II - gas phase reactions of organic species, Atmos. Chem. Phys., 6, 3625-4055, doi:10.5194/acp-6-3625-2006, 2006.

Boy, M., Sogachev, A., Lauros, J., Zhou, L., Guenther, A., and Smolander, S.: SOSA – a new model to simulate the concentrations of organic vapours and sulphuric acid inside the ABL – Part 1: Model description and initial evaluation, Atmos. Chem. Phys., 11, 43-51, doi:10.5194/acp-11-43-2011, 2011.

Chang, C.-C., Wang, J.-L., Candice Lung, S.-C., Chang, C.-Y., Lee, P.-J., Chew, C., Liao, W.-C., Chen, W.-N., and Ou-Yang, C.-F.: Seasonal characteristics of biogenic and anthropogenic isoprene in tropical–subtropical urban environments, Atmos Environ, 99, 298-308, doi:10.1016/j.atmosenv.2014.09.019, 2014.

Chen, W. T., Shao, M., Lu, S. H., Wang, M., Zeng, L. M., Yuan, B., and Liu, Y.: Understanding primary and secondary sources of ambient carbonyl compounds in Beijing using the PMF model, Atmos Chem Phys, 14, 3047-3062, doi:10.5194/acp-14-3047-2014, 2014.

Damian, V., Sandu, A., Damian, M., Potra, F., and Carmichael, G. R.: The kinetic preprocessor KPP-a software environment for solving chemical kinetics, Computers & Chemical Engineering, 26, 1567-1579, doi:10.1016/s0098-1354(02)00128-x, 2002.

Di Carlo, P., Brune, W. H., Martinez, M., Harder, H., Lesher, R., Ren, X., Thornberry, T., Carroll, M. A., Young, V., Shepson, P. B., Riemer, D., Apel, E., and Campbell, C.: Missing OH reactivity in a forest: evidence for unknown reactive biogenic VOCs, Science, 304, 722-725, doi:10.1126/science.1094392, 2004.

Dolgorouky, C., Gros, V., Sarda-Esteve, R., Sinha, V., Williams, J., Marchand, N., Sauvage, S., Poulain, L., Sciare, J., and Bonsang, B.: Total OH reactivity measurements in Paris during the 2010 MEGAPOLI winter campaign, Atmos Chem Phys, 12, 9593-9612, doi:10.5194/acp-12-9593-2012, 2012.

Elshorbany, Y. F., Kurtenbach, R., Wiesen, P., Lissi, E., Rubio, M., Villena, G., Gramsch, E., Rickard, A. R., Pilling, M. J., and Kleffmann, J.: Oxidation capacity of the city air of Santiago, Chile, Atmos Chem Phys, 9, 2257-2273, doi:10.5194/acp-9-2257-2009, 2009.

Elshorbany, Y. F., Kleffmann, J., Hofzumahaus, A., Kurtenbach, R., Wiesen, P., Brauers, T., Bohn, B., Dorn, H. P., Fuchs, H., Holland, F., Rohrer, F., Tillmann, R., Wegener, R., Wahner, A., Kanaya, Y., Yoshino, A., Nishida, S., Kajii, Y., Martinez, M., Kubistin, D., Harder, H., Lelieveld, J., Elste, T., Plass-Dülmer, C., Stange, G., Berresheim, H., and Schurath, U.: HOx budgets during HOxComp: A case study of HOx chemistry under NOx-limited conditions, Journal of Geophysical Research: Atmospheres, 117, doi:10.1029/2011jd017008, 2012.

Ferracci, V., Heimann, I., Abraham, N. L., Pyle, J. A., and Archibald, A. T.: Global modelling of the total OH reactivity: investigations on the “missing” OH sink and its atmospheric implications, Atmos Chem Phys, 18, 7109-7129, doi:10.5194/acp-18-7109-2018, 2018.

Fuchs, H., Tan, Z., Lu, K., Bohn, B., Broch, S., Brown, S. S., Dong, H., Gomm, S., Häseler, R., He, L., Hofzumahaus, A., Holland, F., Li, X., Liu, Y., Lu, S., Min, K.-E., Rohrer, F., Shao, M., Wang, B., Wang, M., Wu, Y., Zeng, L., Zhang, Y., Wahner, A., and Zhang, Y.: OH reactivity at a rural site

(Wangdu) in the North China Plain: contributions from OH reactants and experimental OH budget, Atmos Chem Phys, 17, 645-661, doi:10.5194/acp-17-645-2017, 2017.

Gerasopoulos, E., Kazadzis, S., Vrekoussis, M., Kouvarakis, G., Liakakou, E., Kouremeti, N., Giannadaki, D., Kanakidou, M., Bohn, B., and Mihalopoulos, N.: Factors affecting $O_3$ and $NO_2$ photolysis frequencies measured in the eastern Mediterranean during the five-year period 2002-2006, Journal of Geophysical Research: Atmospheres, 117, doi:10.1029/2012jd017622, 2012.

Geyer, A., Alicke, B., Konrad, S., Schmitz, T., Stutz, J., and Platt, U.: Chemistry and oxidation capacity of the nitrate radical in the continental boundary layer near Berlin, Journal of Geophysical Research: Atmospheres, 106, 8013-8025, doi:10.1029/2000jd900681, 2001.

Geyer, A.: Nighttime formation of peroxy and hydroxyl radicals during the BERLIOZ campaign: Observations and modeling studies, Journal of Geophysical Research, 108, doi:10.1029/2001jd000656, 2003.

Goldstein, A. H., and Galbally, I. E.: Known and unexplored organic constituents in the earth's atmosphere, Environ Sci Technol, 41, 1514-1521, doi:10.1021/es072476p, 2007.

He, Z., Wang, X., Ling, Z., Zhao, J., Guo, H., Shao, M., and Wang, Z.: Contributions of different anthropogenic volatile organic compound sources to ozone formation at a receptor site in the Pearl River Delta region and its policy implications, Atmos. Chem. Phys., 19, 8801-8816, doi:10.5194/acp-19-8801-2019, 2019.

Heard, D. E., and Pilling, M. J.: Measurement of OH and $HO_2$ in the troposphere, Chemical Reviews, 103, 5163-5198, doi:10.1021/cr020522s, 2003.

Jenkin, M. E., Saunders, S. M., and Pilling, M. J.: The tropospheric degradation of volatile organic compounds: a protocol for mechanism development, Atmos Environ, 31, 81-104, doi:10.1016/S1352-2310(96)00105-7, 1997.

Jenkin, M. E., Young, J. C., and Rickard, A. R.: The MCM v3.3.1 degradation scheme for isoprene, Atmos. Chem. Phys., 15, 11433-11459, doi:10.5194/acp-15-11433-2015, 2015.

Kaiser, J., Wolfe, G. M., Bohn, B., Broch, S., Fuchs, H., Ganzeveld, L. N., Gomm, S., Häseler, R., Hofzumahaus, A., Holland, F., Jäger, J., Li, X., Lohse, I., Lu, K., Prévôt, A. S. H., Rohrer, F., Wegener, R., Wolf, R., Mentel, T. F., Kiendler-Scharr, A., Wahner, A., and Keutsch, F. N.: Evidence for an unidentified non-photochemical ground-level source of formaldehyde in the Po Valley with

potential implications for ozone production, Atmos. Chem. Phys., 15, 1289-1298, doi:10.5194/acp-15-1289-2015, 2015.

Kansal, A.: Sources and reactivity of NMHCs and VOCs in the atmosphere: a review, J Hazard Mater, 166, 17-26, doi:10.1016/j.jhazmat.2008.11.048, 2009.

Kim, S., Sanchez, D., Wang, M., Seco, R., Jeong, D., Hughes, S., Barletta, B., Blake, D. R., Jung, J., Kim, D., Lee, G., Lee, M., Ahn, J., Lee, S. D., Cho, G., Sung, M. Y., Lee, Y. H., Kim, D. B., Kim, Y., Woo, J. H., Jo, D., Park, R., Park, J. H., Hong, Y. D., and Hong, J. H.: OH reactivity in urban and suburban regions in Seoul, South Korea - an East Asian megacity in a rapid transition, Faraday Discuss, 189, 231-251, doi:10.1039/c5fd00230c, 2016.

Kovacs, T. A., Brune, W. H., Harder, H., Martinez, M., Simpas, J. B., Frost, G. J., Williams, E., Jobson, T., Stroud, C., Young, V., Fried, A., and Wert, B.: Direct measurements of urban OH reactivity during Nashville SOS in summer 1999, J Environ Monitor, 5, 68-74, doi:10.1039/b204339d, 2003.

Kumar, V., Chandra, B. P., and Sinha, V.: Large unexplained suite of chemically reactive compounds present in ambient air due to biomass fires, Sci Rep-Uk, 8, 626, doi:10.1038/s41598-017-19139-3, 2018.

Lee, J. D., Young, J. C., Read, K. A., Hamilton, J. F., Hopkins, J. R., Lewis, A. C., Bandy, B. J., Davey, J., Edwards, P., Ingham, T., Self, D. E., Smith, S. C., Pilling, M. J., and Heard, D. E.: Measurement and calculation of OH reactivity at a United Kingdom coastal site, J Atmos Chem, 64, 53-76, doi:10.1007/s10874-010-9171-0, 2010.

Li, Z., Xue, L., Yang, X., Zha, Q., Tham, Y. J., Yan, C., Louie, P. K. K., Luk, C. W. Y., Wang, T., and Wang, W.: Oxidizing capacity of the rural atmosphere in Hong Kong, Southern China, Sci Total Environ, 612, 1114-1122, doi:10.1016/j.scitotenv.2017.08.310, 2018.

Liebmann, J., Karu, E., Sobanski, N., Schuladen, J., Ehn, M., Schallhart, S., Quéléver, L., Hellen, H., Hakola, H., Hoffmann, T., Williams, J., Fischer, H., Lelieveld, J., and Crowley, J. N.: Direct measurement of $NO_3$ radical reactivity in a boreal forest, Atmos Chem Phys, 18, 3799-3815, doi:10.5194/acp-18-3799-2018, 2018a.

Liebmann, J. M., Schuster, G., Schuladen, J. B., Sobanski, N., Lelieveld, J., and Crowley, J. N.: Measurement of ambient $NO_3$ reactivity: design, characterization and first deployment of a new

instrument, Atmos Meas Tech, 10, 1241-1258, doi:10.5194/amt-10-1241-2017, 2017.

Liebmann, J. M., Muller, J. B. A., Kubistin, D., Claude, A., Holla, R., Plass-Dülmer, C., Lelieveld, J., and Crowley, J. N.: Direct measurements of $NO_3$ reactivity in and above the boundary layer of a mountaintop site: identification of reactive trace gases and comparison with OH reactivity, Atmos Chem Phys, 18, 12045-12059, doi:10.5194/acp-18-12045-2018, 2018b.

Liu, C. T., Ma, Z. B., Mu, Y. J., Liu, J. F., Zhang, C. L., Zhang, Y. Y., Liu, P. F., and Zhang, H. X.: The levels, variation characteristics, and sources of atmospheric non-methane hydrocarbon compounds during wintertime in Beijing, China, Atmos Chem Phys, 17, 10633-10649, doi:10.5194/acp-17-10633-2017, 2017.

Liu, Y., Shao, M., Kuster, W. C., Goldan, P. D., Li, X., Lu, S., and de Gouw, J. A.: Source identification of reactive hydrocarbons and oxygenated VOCs in the summertime in Beijing, Environ Sci Technol, 43, 75-81, doi:10.1021/es801716n, 2009.

Lou, S., Holland, F., Rohrer, F., Lu, K., Bohn, B., Brauers, T., Chang, C. C., Fuchs, H., Häseler, R., Kita, K., Kondo, Y., Li, X., Shao, M., Zeng, L., Wahner, A., Zhang, Y., Wang, W., and Hofzumahaus, A.: Atmospheric OH reactivities in the Pearl River Delta – China in summer 2006: measurement and model results, Atmos Chem Phys, 10, 11243-11260, doi:10.5194/acp-10-11243-2010, 2010.

Lu, K., Zhang, Y., Su, H., Brauers, T., Chou, C. C., Hofzumahaus, A., Liu, S. C., Kita, K., Kondo, Y., Shao, M., Wahner, A., Wang, J., Wang, X., and Zhu, T.: Oxidant ($O_3$+ $NO_2$) production processes and formation regimes in Beijing, Journal of Geophysical Research, 115, doi:10.1029/2009jd012714, 2010.

Lu, K., Guo, S., Tan, Z., Wang, H., Shang, D., Liu, Y., Li, X., Wu, Z., Hu, M., and Zhang, Y.: Exploring the Atmospheric Free Radical chemistry in China: The Self-Cleansing Capacity and the Formation of Secondary air Pollution, National Science Review, doi:10.1093/nsr/nwy073, 2018.

Lu, K., Fuchs, H., Hofzumahaus, A., Tan, Z., Wang, H., Zhang, L., Schmitt, S. H., Rohrer, F., Bohn, B., Broch, S., Dong, H., Gkatzelis, G. I., Hohaus, T., Holland, F., Li, X., Liu, Y., Liu, Y., Ma, X., Novelli, A., Schlag, P., Shao, M., Wu, Y., Wu, Z., Zeng, L., Hu, M., Kiendler-Scharr, A., Wahner, A., and Zhang, Y.: Fast Photochemistry in Wintertime Haze: Consequences for Pollution Mitigation Strategies, Environ Sci Technol, 53, 10676-10684, doi:10.1021/acs.est.9b02422, 2019.

Lu, K. D., Hofzumahaus, A., Holland, F., Bohn, B., Brauers, T., Fuchs, H., Hu, M., Häseler, R., Kita,

K., Kondo, Y., Li, X., Lou, S. R., Oebel, A., Shao, M., Zeng, L. M., Wahner, A., Zhu, T., Zhang, Y. H., and Rohrer, F.: Missing OH source in a suburban environment near Beijing: observed and modelled OH and $HO_2$ concentrations in summer 2006, Atmos. Chem. Phys., 13, 1057-1080, doi:10.5194/acp-13-1057-2013, 2013.

Lyu, X., Wang, N., Guo, H., Xue, L., Jiang, F., Zeren, Y., Cheng, H., Cai, Z., Han, L., and Zhou, Y.: Causes of a continuous summertime $O_3$ pollution event in Jinan, a central city in the North China Plain, Atmos Chem Phys, 19, 3025-3042, doi:10.5194/acp-19-3025-2019, 2019.

Mao, J., Ren, X., Chen, S., Brune, W. H., Chen, Z., Martinez, M., Harder, H., Lefer, B., Rappenglück, B., Flynn, J., and Leuchner, M.: Atmospheric oxidation capacity in the summer of Houston 2006: Comparison with summer measurements in other metropolitan studies, Atmos Environ, 44, 4107-4115, doi:10.1016/j.atmosenv.2009.01.013, 2010.

Mogensen, D., Smolander, S., Sogachev, A., Zhou, L., Sinha, V., Guenther, A., Williams, J., Nieminen, T., Kajos, M. K., and Rinne, J.: Modelling atmospheric OH-reactivity in a boreal forest ecosystem, Atmospheric Chemistry & Physics, 11, 9709-9719, doi:10.5194/acp-11-9709-2011, 2011.

Mogensen, D., Gierens, R., Crowley, J. N., Keronen, P., and Smolander, S.: Simulations of atmospheric OH, $O_3$ and $NO_3$ reactivities within and above the boreal forest, Atmospheric Chemistry & Physics, 15, 3909-3932, doi:10.5194/acp-15-3909-2015, 2015.

Praplan, A. P., Pfannerstill, E. Y., Williams, J., and Hellén, H.: OH reactivity of the urban air in Helsinki, Finland, during winter, Atmos Environ, 169, 150-161, doi:10.1016/j.atmosenv.2017.09.013, 2017.

Ren, X.: HOx concentrations and OH reactivity observations in New York City during PMTACS-NY2001, Atmos Environ, 37, 3627-3637, doi:10.1016/s1352-2310(03)00460-6, 2003.

Ren, X., Brune, W. H., Mao, J., Mitchell, M. J., Lesher, R. L., Simpas, J. B., Metcalf, A. R., Schwab, J. J., Cai, C., and Li, Y.: Behavior of OH and $HO_2$ in the winter atmosphere in New York City, Atmos Environ, 40, 252-263, doi:10.1016/j.atmosenv.2005.11.073, 2006a.

Ren, X., Brune, W. H., Oliger, A., Metcalf, A. R., Simpas, J. B., Shirley, T., Schwab, J. J., Bai, C., Roychowdhury, U., Li, Y., Cai, C., Demerjian, K. L., He, Y., Zhou, X., Gao, H., and Hou, J.: OH, $HO_2$, and OH reactivity during the PMTACS-NY Whiteface Mountain 2002 campaign:

Observations and model comparison, Journal of Geophysical Research: Atmospheres, 111, doi:10.1029/2005jd006126, 2006b.

Sadanaga, Y., Yoshino, A., Kato, S., and Kajii, Y.: Measurements of OH reactivity and photochemical ozone production in the urban atmosphere, Environ Sci Technol, 39, 8847-8852, doi:10.1021/es049457p, 2005.

Salgado, M. S., Monedero, E., Villanueva, F., Martín, P., Tapia, A., and Caba?as, B.: Night-Time Atmospheric Fate of Acrolein and Crotonaldehyde, Environ Sci Technol, 42, 2394-2400, doi:10.1021/es702533u, 2008.

Saunders, S. M., Jenkin, M. E., Derwent, R. G., and Pilling, M. J.: Protocol for the development of the Master Chemical Mechanism, MCM v3 (Part A): tropospheric degradation of non-aromatic volatile organic compounds, Atmos. Chem. Phys., 3, 161-180, doi:10.5194/acp-3-161-2003, 2003.

Shirley, T. R., Brune, W. H., Ren, X., Mao, J., Lesher, R., Cardenas, B., Volkamer, R., Molina, L. T., Molina, M. J., Lamb, B., Velasco, E., Jobson, T., and Alexander, M.: Atmospheric oxidation in the Mexico City Metropolitan Area (MCMA) during April 2003, Atmos Chem Phys, 6, 2753-2765, doi:10.5194/acp-6-2753-2006, 2006.

Sinha, V., Williams, J., Crowley, J. N., and Lelieveld, J.: The Comparative Reactivity Method – a new tool to measure total OH Reactivity in ambient air, Atmos. Chem. Phys., 8, 2213-2227, doi:10.5194/acp-8-2213-2008, 2008.

Song, M. D., Tan, Q. W., Feng, M., Qu, Y., Liu, X. G., An, J. L., and Zhang, Y. H.: Source Apportionment and Secondary Transformation of Atmospheric Nonmethane Hydrocarbons in Chengdu, Southwest China, J Geophys Res-Atmos, 123, 9741-9763, doi:10.1029/2018jd028479, 2018.

Tan, Z., Fuchs, H., Lu, K., Hofzumahaus, A., Bohn, B., Broch, S., Dong, H., Gomm, S., Häseler, R., He, L., Holland, F., Li, X., Liu, Y., Lu, S., Rohrer, F., Shao, M., Wang, B., Wang, M., Wu, Y., Zeng, L., Zhang, Y., Wahner, A., and Zhang, Y.: Radical chemistry at a rural site (Wangdu) in the North China Plain: observation and model calculations of OH, $HO_2$ and $RO_2$ radicals, Atmos. Chem. Phys., 17, 663-690, doi:10.5194/acp-17-663-2017, 2017.

Tan, Z., Lu, K., Jiang, M., Su, R., Wang, H., Lou, S., Fu, Q., Zhai, C., Tan, Q., Yue, D., Chen, D., Wang, Z., Xie, S., Zeng, L., and Zhang, Y.: Daytime atmospheric oxidation capacity in four Chinese

megacities during the photochemically polluted season: a case study based on box model simulation, Atmos Chem Phys, 19, 3493-3513, doi:10.5194/acp-19-3493-2019, 2019.

Tong, S., Hou, S., Zhang, Y., Chu, B., Liu, Y., He, H., Zhao, P., and Ge, M.-F.: Exploring the nitrous acid (HONO) formation mechanism in winter Beijing: direct emissions and heterogeneous production in urban and suburban areas, Faraday Discuss., 189, doi:10.1039/C5FD00163C, 2015.

Wang, W., Li, X., Shao, M., Hu, M., Zeng, L., Wu, Y., and Tan, T.: The impact of aerosols on photolysis frequencies and ozone production in Beijing during the 4-year period 2012–2015, Atmos Chem Phys, 19, 9413-9429, doi:10.5194/acp-19-9413-2019, 2019.

Wang, Y., Hu, B., Tang, G., Ji, D., Zhang, H., Bai, J., Wang, X., and Wang, Y.: Characteristics of ozone and its precursors in Northern China: A comparative study of three sites, Atmos Res, 132-133, 450-459, doi:10.1016/j.atmosres.2013.04.005, 2013.

Wang, Y., Riva, M., Xie, H., Heikkinen, L., Schallhart, S., Zha, Q., Yan, C., He, X. C., Peräkylä, O., and Ehn, M.: Formation of highly oxygenated organic molecules from chlorine-atom-initiated oxidation of alpha-pinene, Atmos. Chem. Phys., 20, 5145-5155, doi:10.5194/acp-20-5145-2020, 2020.

Whalley, L. K., Stone, D., Bandy, B., Dunmore, R., Hamilton, J. F., Hopkins, J., Lee, J. D., Lewis, A. C., and Heard, D. E.: Atmospheric OH reactivity in central London: observations, model predictions and estimates of in situ ozone production, Atmos Chem Phys, 16, 2109-2122, doi:10.5194/acp-16-2109-2016, 2016.

Wu, R., Li, J., Hao, Y., Li, Y., Zeng, L., and Xie, S.: Evolution process and sources of ambient volatile organic compounds during a severe haze event in Beijing, China, Sci Total Environ, 560-561, 62-72, doi:10.1016/j.scitotenv.2016.04.030, 2016.

Xu, J., Ma, J. Z., Zhang, X. L., Xu, X. B., Xu, X. F., Lin, W. L., Wang, Y., Meng, W., and Ma, Z. Q.: Measurements of ozone and its precursors in Beijing during summertime: impact of urban plumes on ozone pollution in downwind rural areas, Atmos Chem Phys, 11, 12241-12252, doi:10.5194/acp-11-12241-2011, 2011.

Xue, L., Gu, R., Wang, T., Wang, X., Saunders, S., Blake, D., Louie, P. K. K., Luk, C. W. Y., Simpson, I., Xu, Z., Wang, Z., Gao, Y., Lee, S., Mellouki, A., and Wang, W.: Oxidative capacity and radical chemistry in the polluted atmosphere of Hong Kong and Pearl River Delta region: analysis of a

842 severe photochemical smog episode, Atmos Chem Phys, 16, 9891-9903, doi:10.5194/acp-16-9891-
843 2016, 2016.
844 Yang, Y., Shao, M., Wang, X., Nölscher, A. C., Kessel, S., Guenther, A., and Williams, J.: Towards
845 a quantitative understanding of total OH reactivity: A review, Atmos Environ, 134, 147-161,
846 doi:10.1016/j.atmosenv.2016.03.010, 2016.
847 Yang, Y., Shao, M., Keßel, S., Li, Y., Lu, K., Lu, S., Williams, J., Zhang, Y., Zeng, L., Nölscher, A.
848 C., Wu, Y., Wang, X., and Zheng, J.: How the OH reactivity affects the ozone production efficiency:
849 case studies in Beijing and Heshan, China, Atmos Chem Phys, 17, 7127-7142, doi:10.5194/acp-17-
850 7127-2017, 2017.
851 Yang, Y., Ji, D., Sun, J., Wang, Y., Yao, D., Zhao, S., Yu, X., Zeng, L., Zhang, R., Zhang, H., Wang,
852 Y., and Wang, Y.: Ambient volatile organic compounds in a suburban site between Beijing and
853 Tianjin: Concentration levels, source apportionment and health risk assessment, Sci Total Environ,
854 695, 133889, doi:10.1016/j.scitotenv.2019.133889, 2019.
855 Ye, Y., Galbally, I., and Weeks, I.: Emission of 1,3-butadiene from petrol-driven motor vehicles,
856 Atmos Environ, 31, 1157-1165, doi:10.1016/S1352-2310(96)00308-1, 1997.
857 Yoshino, A., Sadanaga, Y., Watanabe, K., Kato, S., Miyakawa, Y., Matsumoto, J., and Kajii, Y.:
858 Measurement of total OH reactivity by laser-induced pump and probe technique—comprehensive
859 observations in the urban atmosphere of Tokyo, Atmos Environ, 40, 7869-7881,
860 doi:10.1016/j.atmosenv.2006.07.023, 2006.
861 Yuan, B., Shao, M., de Gouw, J., Parrish, D. D., Lu, S., Wang, M., Zeng, L., Zhang, Q., Song, Y.,
862 Zhang, J., and Hu, M.: Volatile organic compounds (VOCs) in urban air: How chemistry affects the
863 interpretation of positive matrix factorization (PMF) analysis, Journal of Geophysical Research:
864 Atmospheres, 117, 24302, doi:10.1029/2012jd018236, 2012.
865 Yuan, B., Hu, W. W., Shao, M., Wang, M., Chen, W. T., Lu, S. H., Zeng, L. M., and Hu, M.: VOC
866 emissions, evolutions and contributions to SOA formation at a receptor site in eastern China, Atmos
867 Chem Phys, 13, 8815-8832, doi:10.5194/acp-13-8815-2013, 2013.
868 Yuan, Z. B., Lau, A. K. H., Shao, M., Louie, P. K. K., Liu, S. C., and Zhu, T.: Source analysis of
869 volatile organic compounds by positive matrix factorization in urban and rural environments in
870 Beijing, J Geophys Res-Atmos, 114, doi:10.1029/2008JD011190, 2009.

Zannoni, N., Gros, V., Sarda Esteve, R., Kalogridis, C., Michoud, V., Dusanter, S., Sauvage, S., Locoge, N., Colomb, A., and Bonsang, B.: Summertime OH reactivity from a receptor coastal site in the Mediterranean Basin, Atmos Chem Phys, 17, 12645-12658, doi:10.5194/acp-17-12645-2017, 2017.

Zhang, W., Tong, S., Ge, M.-F., An, J., Shi, Z., Hou, S., Xia, K., qu, y., Zhang, H., Chu, B., Sun, Y., and He, H.: Variations and sources of nitrous acid (HONO) during a severe pollution episode in Beijing in winter 2016, Sci Total Environ, 648, doi:10.1016/j.scitotenv.2018.08.133, 2019.

Zheng, H., Kong, S. F., Xing, X. L., Mao, Y., Hu, T. P., Ding, Y., Li, G., Liu, D. T., Li, S. L., and Qi, S. H.: Monitoring of volatile organic compounds (VOCs) from an oil and gas station in northwest China for 1 year, Atmos Chem Phys, 18, 4567-4595, doi:10.5194/acp-18-4567-2018, 2018.

Zhou, P., Ganzeveld, L., Rannik, ü., Zhou, L., Gierens, R., Taipale, D., Mammarella, I., and Boy, M.: Simulating ozone dry deposition at a boreal forest with a multi-layer canopy deposition model, Atmospheric Chemistry & Physics, 17, 1361-1379, doi:10.5194/acp-17-1361-2017, 2017a.

Zhou, P., Ganzeveld, L., Taipale, D., Rannik, Ü., Rantala, P., Rissanen, M. P., Chen, D., and Boy, M.: Boreal forest BVOC exchange: emissions versus in-canopy sinks, Atmos. Chem. Phys., 17, 14309-14332, doi:10.5194/acp-17-14309-2017, 2017b.

Zhu, J., Wang, S., Wang, H., Jing, S., Lou, S., Saiz-Lopez, A., and Zhou, B.: Observationally constrained modeling of atmospheric oxidation capacity and photochemical reactivity in Shanghai, China, Atmos. Chem. Phys., 20, 1217-1232, doi:10.5194/acp-20-1217-2020, 2020.

899 **Figure captions**

900

901

902

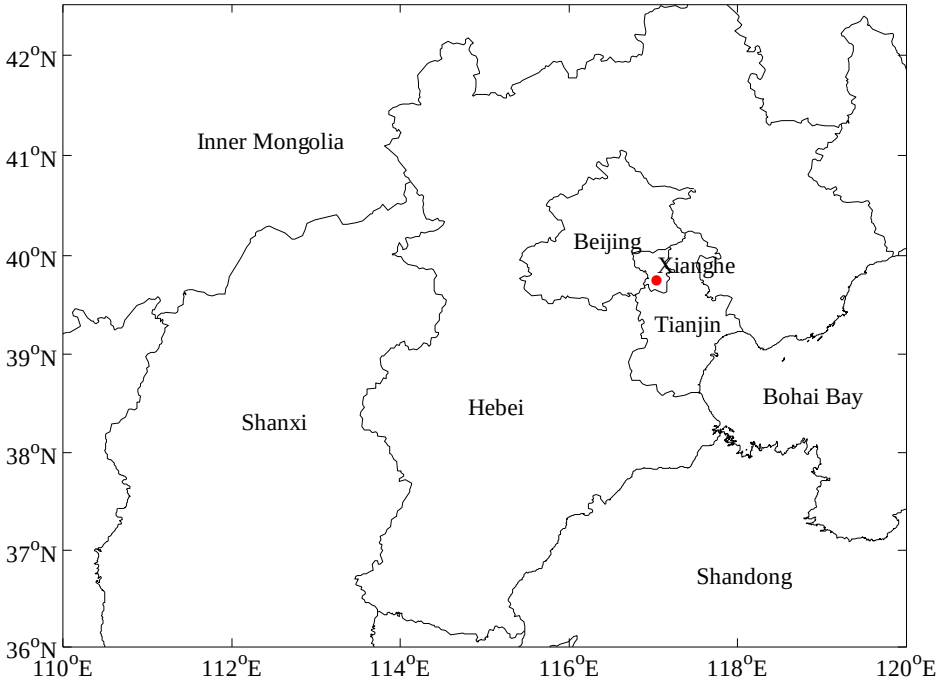


903 Figure 1. The location of the sampling site, which is marked with a red dot. The blacklines are
904 provincial boundary lines of each province. (The figure was produced by MATLAB 2017a).

905

906

907

908

909

910

911

912

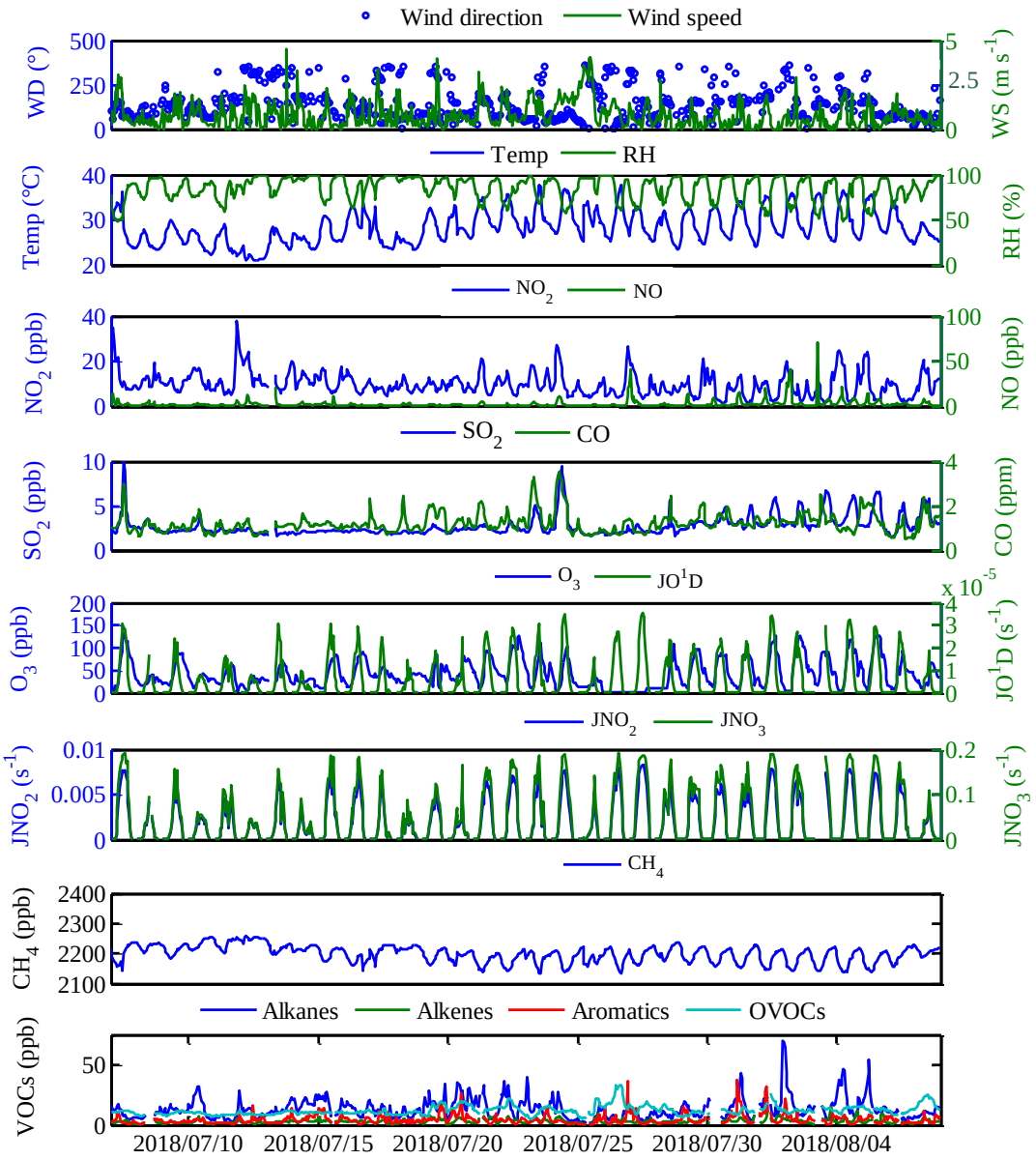


Figure 2. Time series of meteorology parameters, trace gases, photolysis rates and VOCs concentrations during the field campaign at Xianghe from 6 July to 6 August 2018.

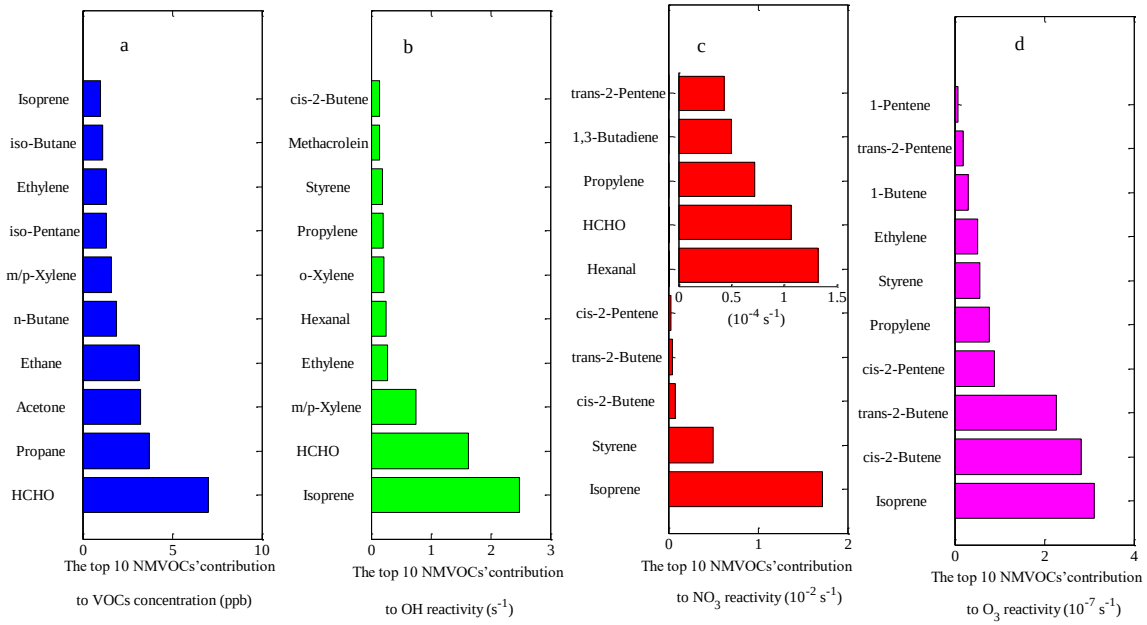


Figure 3. The top 10 NMVOCs' contribution to total NMVOCs concentration (a), OH reactivity (b), $NO_3$ reactivity (c) and $O_3$ reactivity (d) during the field campaign at Xianghe from 6 July to 6 August 2018.

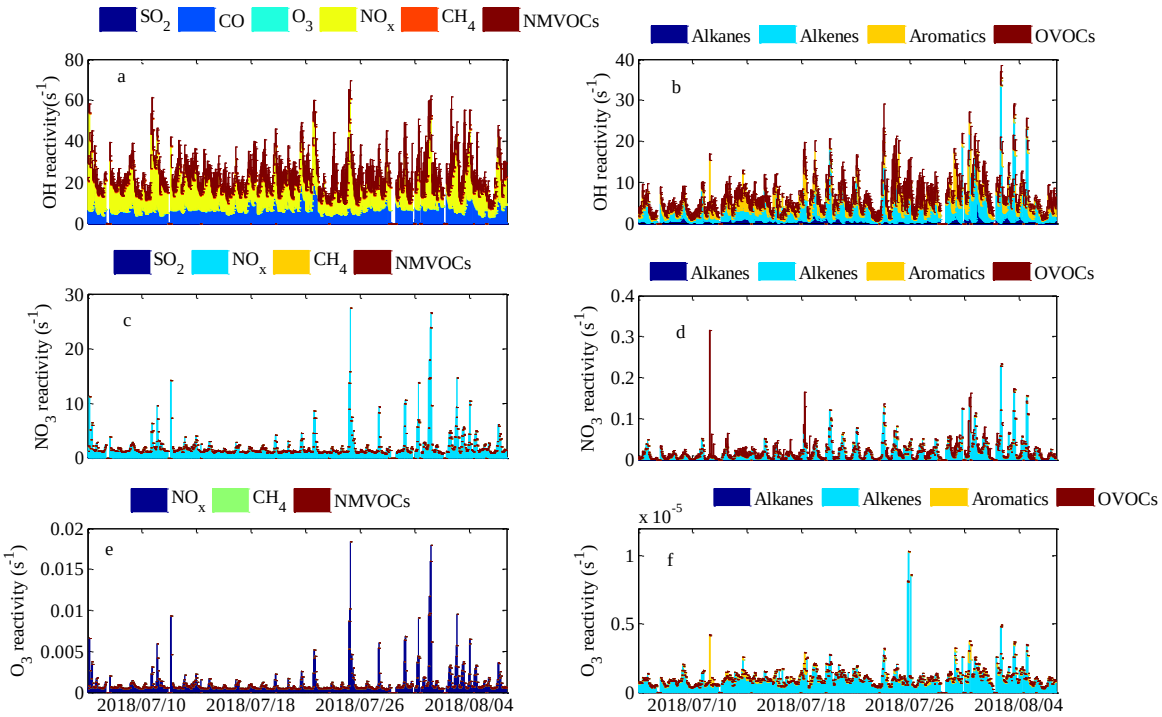


Figure 4. The time series of OH reactivity (a,b), $NO_3$ reactivity (c,d) and $O_3$ reactivity (e,f) during the field campaign at Xianghe from 6 July to 6 August 2018.

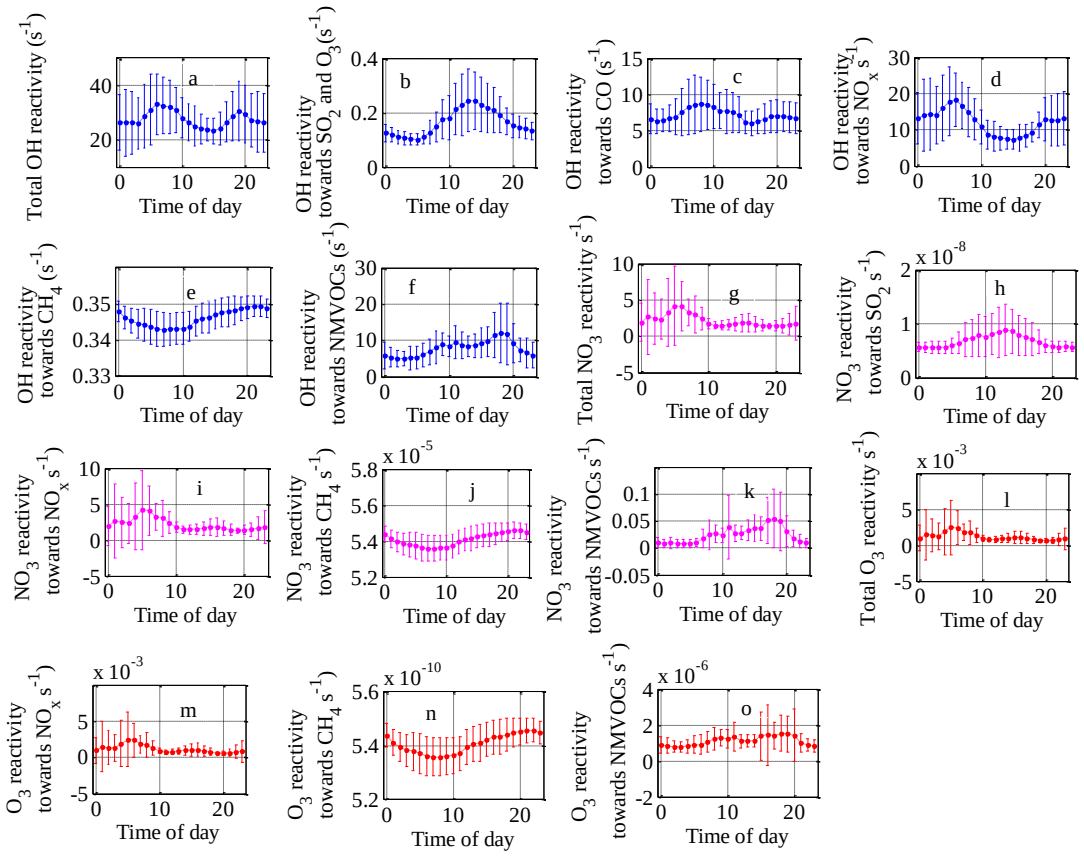


Figure 5. Mean diurnal variations of OH reactivity (a-f), $NO_3$ reactivity (g-k) and $O_3$ reactivity (l-o) of trace gases during the field campaign at Xianghe from 6 July to 6 August 2018.

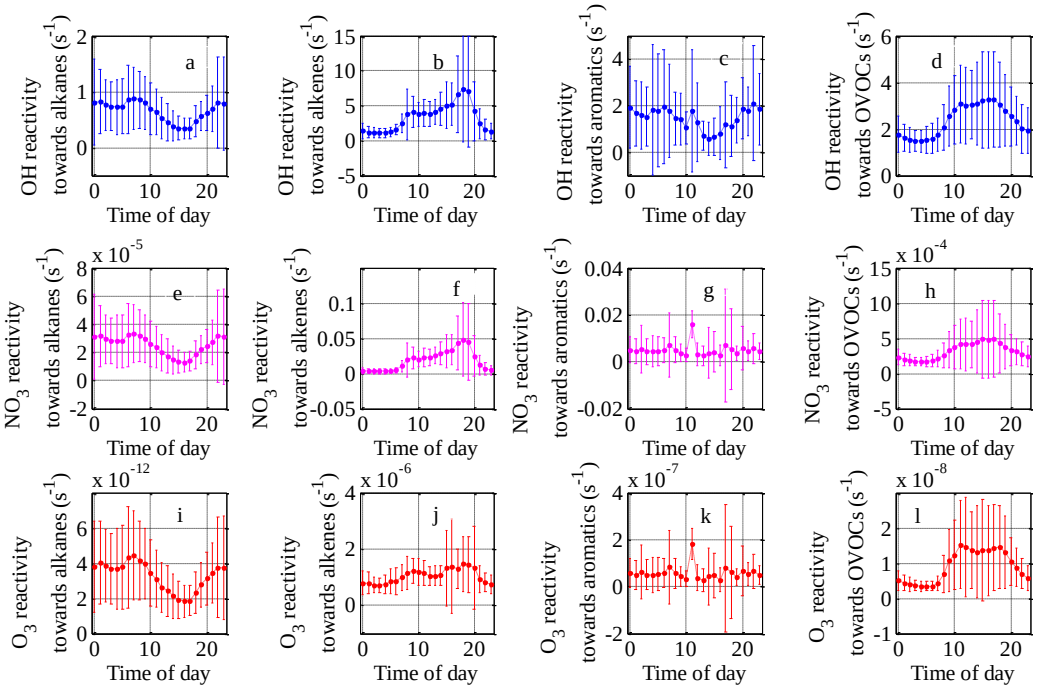


Figure 6. Mean diurnal variations of OH reactivity (a-d), $NO_3$ reactivity (e-h) and $O_3$ reactivity (i-l) of NMVOCs groups during the field campaign at Xianghe from 6 July to 6 August 2018.

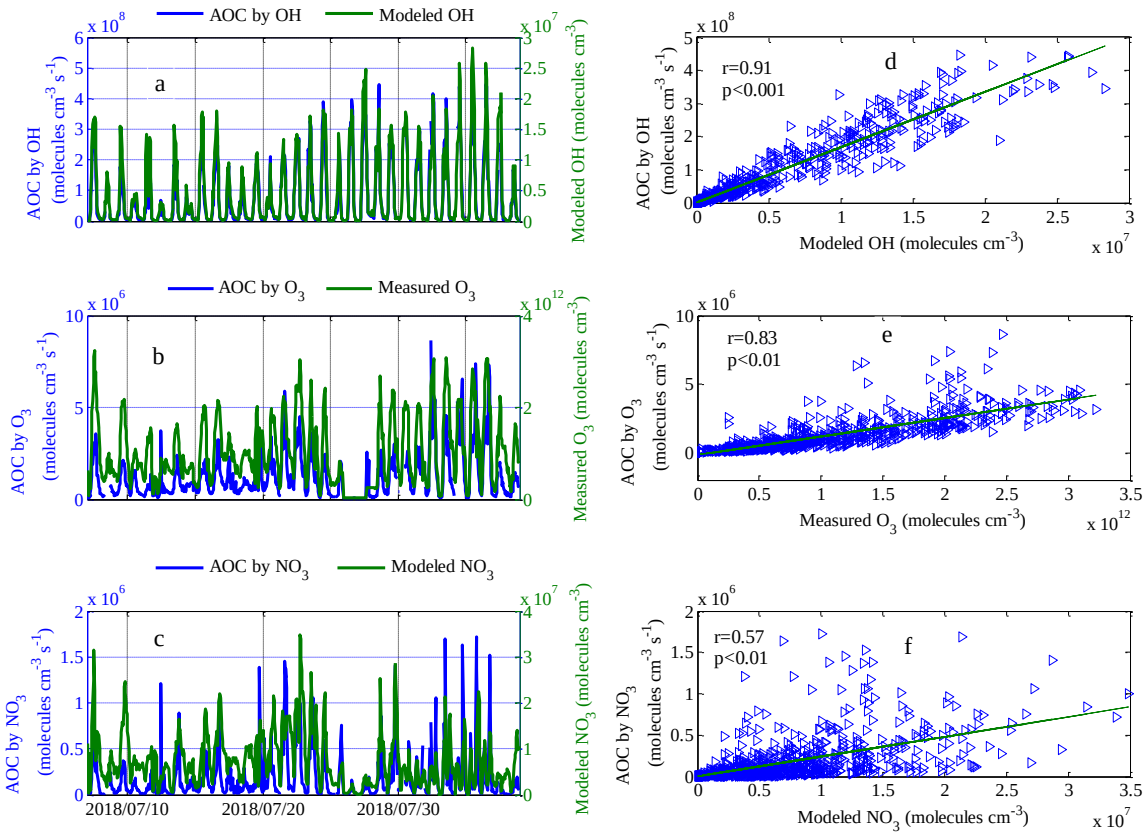


Figure 7. Comparisons of calculated AOC by modeled OH (a), measured $O_3$ (b) and modeled $NO_3$ (c), and corresponding oxidation concentrations. The left column shows the time series and the right column shows scatterplots of calculated AOC and corresponding oxidation concentrations. Note: r and p are the correlation coefficient and the significance level, respectively.

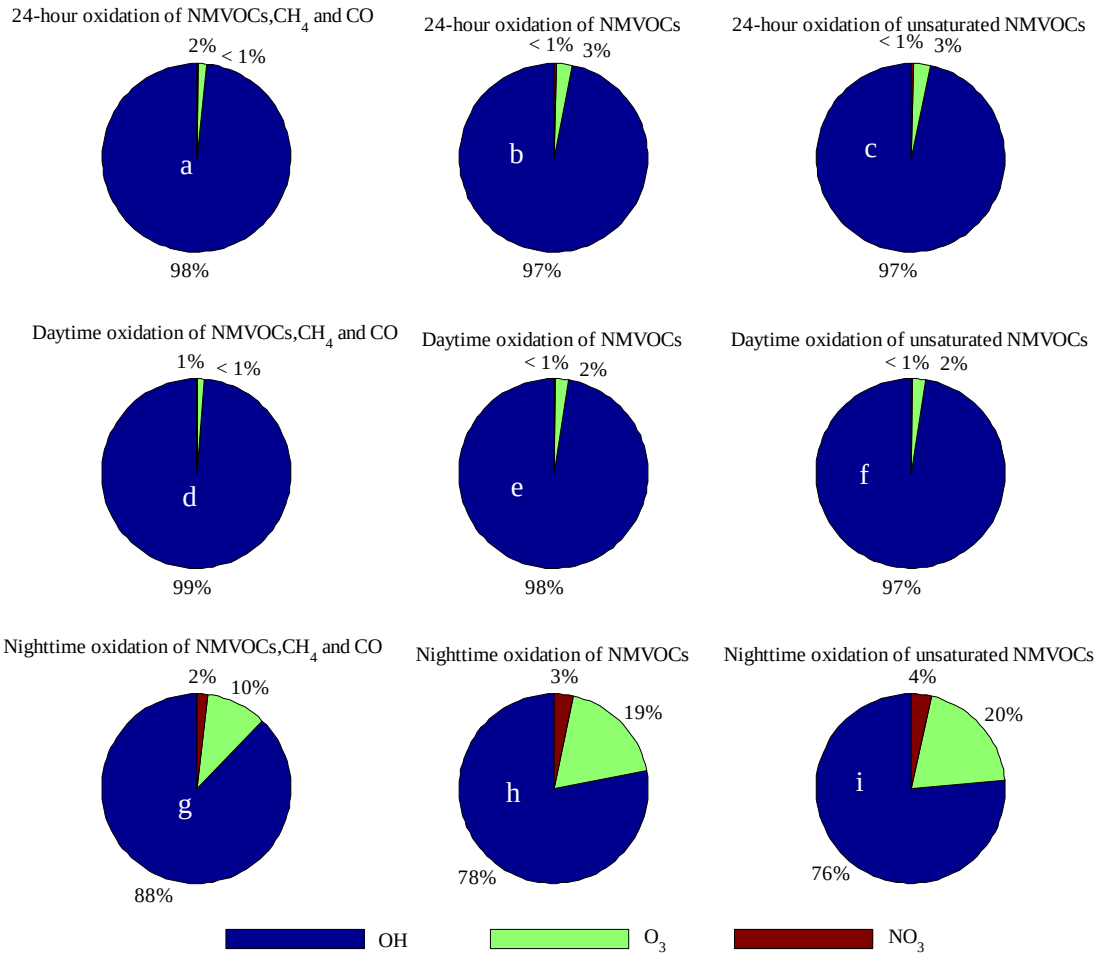


Figure 8. Comparison of the relative contributions of OH, $NO_3$ and $O_3$ to the 24-h, daytime and nighttime averaged loss rates. Data are calculated for the loss rates of (a, d and g) NMVOCs, $CH_4$ and CO, (b,e and h) NMVOCs only, and (c,f and i) unsaturated NMVOCs only.

1013 **Table captions**

1014 Table1. Comparison of speciated OH reactivity with former studies in China.

| Species | This study | Beijing[a] | Shangdianzi[a] | Heshan[b] | Guangzhou[c] | Chongqing[c] | Beijing[d] | Shanghai[e] |
|---|---|---|---|---|---|---|---|---|
| $CH_4$ | 0.346 | | | | | | | 0.34 |
| Ethane | 0.019 | 0.01 | 0.01 | 0.023 | 0.24 | 0.59 | | |
| Propane | 0.100 | 0.32 | 0.10 | 0.081 | | | | |
| iso-Butane | 0.058 | 0.45 | 0.12 | 0.075 | | | | |
| n-Butane | 0.111 | 0.09 | 0.08 | 0.104 | | | | |
| Cyclopentane | 0.001 | 0.08 | 0.03 | 0.011 | | | | |
| iso-Pentane | 0.119 | 1.18 | 0.25 | 0.168 | | | | |
| n-Pentane | 0.067 | 0.60 | 0.16 | 0.136 | | | | |
| 2,2-Dimethylbutane | 0.002 | 0.08 | 0.08 | 0.003 | | | | |
| 2,3-Dimethylbutane | 0.017 | 0.23 | 0.11 | 0.013 | | | | |
| 2-Methylpentane | 0.016 | 0.56 | 0.10 | 0.077 | | | | |
| 3-Methylpentane | 0.018 | 0.44 | 0.10 | 0.047 | | | | |
| n-Hexane | 0.020 | 0.60 | 0.08 | 0.055 | | | | |
| 2,4-Dimethylpentane | 0.001 | | | 0.069 | | | | |
| Methylcyclopentane | 0.019 | 0.49 | 0.07 | 0.024 | | | | |
| 2-Methylhexane | 0.003 | 0.22 | 0.04 | 0.035 | | | | |
| 2,3-Dimethylpentane | 0.001 | | 0.00 | 0.007 | | | | |
| Cyclohexane | 0.048 | 0.26 | 0.05 | 0.015 | | | | |
| 3-Methylhexane | 0.004 | 0.28 | 0.05 | 0.039 | | | | |
| 2,2,4-Trimethylpentane | 0.002 | 0.04 | 0.01 | 0.036 | | | | |
| n-Heptane | 0.006 | 0.24 | 0.04 | 0.033 | | | | |
| Methylcyclohexane | 0.003 | 0.25 | 0.03 | 0.015 | | | | |
| 2,3,4-Trimethylpentane | 0.001 | 0.03 | 0.01 | 0.031 | | | | |
| 2-Methylheptane | 0.002 | - | 0.00 | 0.007 | | | | |
| 3-Methylheptane | 0.001 | 0.11 | 0.03 | 0.007 | | | | |
| n-Octane | 0.004 | 0.38 | 0.11 | 0.014 | | | | |
| Nonane | 0.004 | 0.19 | 0.03 | 0.010 | | | | |
| n-Decane | 0.003 | | | 0.008 | | | | |
| n-Undecane | 0.002 | | | 0.006 | | | | |
| Ethylene | 0.273 | 0.35 | 0.18 | 0.617 | 0.29 | 0.73 | | |
| Propylene | 0.202 | 4.86 | 1.00 | 0.464 | 0.40 | 0.52 | | |
| trans-2-Butene | 0.067 | 1.98 | 0.31 | 0.063 | | | | |
| 1-Butene | 0.100 | 1.65 | 0.73 | 0.077 | | | | |
| cis-2-Butene | 0.145 | 1.33 | 0.32 | 0.084 | | | | |
| 1,3-Butadiene | 0.034 | - | - | - | | | | |
| 1-Pentene | 0.023 | 0.50 | 0.22 | 1.136 | | | | |
| trans-2-Pentene | 0.006 | 0.64 | 0.13 | 0.066 | 0.31 | 0.26 | | |
| cis-2-Pentene | 0.034 | 1.20 | 0.29 | 0.080 | | | | |
| Isoprene | 2.463 | 5.59 | 2.81 | 0.862 | 0.31 | 0.92 | | |

| | | | | | | | | |
|---|---|---|---|---|---|---|---|---|
| 1-Hexene | 0.007 | - | - | 0.018 | | | | |
| HCHO | 1.797 | | | 1.153 | | | | |
| Acrolein | 0.027 | | | 0.009 | | | | |
| Propanal | 0.067 | | | 0.139 | | | | |
| Acetone | 0.013 | | | 0.010 | | | | |
| MTBE | 0.009 | | | - | | | | |
| Methacrolein | 0.146 | | | 0.072 | | | | |
| n-Butanal | 0.024 | | | 0.059 | | | | |
| MethylVinylKetone | 0.138 | | | 0.039 | | | | |
| Methylethylketone | 0.014 | | | 0.020 | | | | |
| 2-Pentanone | 0.001 | | | 0.001 | | | | |
| Pentanal | 0.042 | | | 0.028 | | | | |
| 3-Pentanone | 0.001 | | | 0.002 | | | | |
| Hexanal | 0.247 | | | 0.055 | | | | |
| Benzene | 0.017 | 0.34 | 0.13 | 0.030 | | | | |
| Toluene | 0.092 | 2.22 | 0.39 | 0.518 | 0.73 | 0.15 | | |
| Ethylbenzene | 0.085 | 0.88 | 0.18 | 0.188 | | | | |
| m/p-Xylene | 0.749 | 3.05 | 0.43 | 0.754 | 0.74 | 0.31 | | |
| o-Xylene | 0.216 | 0.93 | 0.12 | 0.194 | 0.35 | 0.10 | | |
| Styrene | 0.193 | 0.34 | 014 | 0.900 | 0.26 | 0.16 | | |
| Isopropylbenzene | 0.002 | 0.04 | 0.01 | 0.004 | | | | |
| n-Propylbenzene | 0.002 | 0.25 | 0.16 | 0.004 | | | | |
| m-Ethyltoluene | 0.016 | | | 0.026 | | | | |
| p-Ethyltoluene | 0.013 | | | 0.027 | | | | |
| 1,3,5-Trimethylbenzene | 0.031 | 2.90 | 1.08 | 0.042 | | | | |
| o-Ethyltoluene | 0.006 | | | 0.018 | | | | |
| 1,2,4-Trimethylbenzene | 0.028 | | | 0.080 | 0.16 | 0.17 | | |
| 1,2,3-Trimethylbenzene | 0.008 | | | 0.028 | | | | |
| CO | 7.196 | 6.90 | 5.37 | | | | 9.13 | 3.15 |
| NO | 2.139 | | | | | | 0.58 | 0.78 |
| $NO_2$ | 9.947 | | | | | | 4.08 | 2.87 |
| $SO_2$ | 0.088 | | | | | | 0.33 | |
| $O_3$ | 0.076 | | | | | | | |

[a] (Xu et al., 2011); [b] (Yang et al., 2017); [c] (Tan et al., 2019); [d] (Liu et al., 2009); [e] (Zhu et al., 2020).

Table 2. The top 10 NMVOCs species in terms of concentration (first column), OH reactivity (second column), $NO_3$ reactivity (third column) and $O_3$ reactivity (fourth column) and their corresponding contributions to concentration, OH, $NO_3$ and $O_3$ reactivity towards NMVOCs (%).

| **First column** | | | | | **Second column** | | | | |
|---|---|---|---|---|---|---|---|---|---|
| **Species** | **Concentration** | OH reactivity | $NO_3$ reactivity | $O_3$ reactivity | **Species** | **Concentration** | OH reactivity | $NO_3$ reactivity | $O_3$ reactivity |
| HCHO | **22.3** | 30.3 | 1.5 | 0.2 | HCHO | 22.3 | **30.3** | 1.5 | 0.2 |
| Propane | **11.8** | 1.9 | 0.1 | 0.0 | m/p-Xylene | 5.1 | **14.0** | 0.1 | 0.0 |
| Acetone | **10.2** | 0.3 | 0.0 | 0.1 | Ethylene | 4.2 | **5.0** | 0.1 | 6.1 |
| Ethane | **6.0** | 0.4 | 0.0 | 0.0 | Hexanal | 1.1 | **4.6** | 1.9 | 0.0 |
| n-Butane | **5.1** | 2.1 | 0.0 | 0.1 | o-Xylene | 2.1 | **4.0** | 0.1 | 0.0 |
| m/p-Xylene | **4.3** | 14.0 | 0.1 | 0.1 | Propylene | 1.0 | **3.7** | 1.0 | 9.0 |
| iso-Pentane | **4.2** | 2.2 | 0.1 | 0.1 | Styrene | 0.4 | **3.6** | 70.2 | 6.6 |
| Ethylene | **4.4** | 5.0 | 0.1 | 6.1 | Methacrolein | 0.7 | **2.7** | 0.2 | 0.7 |
| iso-Butane | **3.5** | 1.1 | 0.0 | 0.0 | cis-2-Butene | 0.3 | **2.7** | 11.2 | 33.0 |
| n-Pentane | **2.3** | 1.3 | 0.0 | 0.0 | MethylVinylKetone | 0.9 | **2.6** | 0.1 | 0.0 |
| **Third column** | | | | | **Forth column** | | | | |
| **Species** | **Concentration** | OH reactivity | $NO_3$ reactivity | $O_3$ reactivity | **Species** | **Concentration** | OH reactivity | $NO_3$ reactivity | $O_3$ reactivity |
| Styrene | 0.4 | 3.6 | **70.2** | 6.6 | cis-2-Butene | 0.3 | 2.7 | 11.2 | **33.0** |
| cis-2-Butene | 0.3 | 2.7 | **11.2** | 33.0 | trans-2-Butene | 0.2 | 1.3 | 6.6 | **26.5** |
| trans-2-Butene | 0.2 | 1.3 | **6.6** | 26.5 | cis-2-Pentene | 0.1 | 0.8 | 3.5 | **10.3** |
| cis-2-Pentene | 0.1 | 0.8 | **3.5** | 10.3 | Propylene | 1.0 | 3.7 | 1.0 | **9.0** |
| Hexanal | 1.1 | 4.6 | **1.9** | 0.0 | Styrene | 0.4 | 3.6 | 70.2 | **6.6** |
| HCHO | 22.3 | 30.3 | **1.5** | 0.2 | Ethylene | 4.2 | 5.0 | 0.1 | **6.1** |
| Propylene | 1.0 | 3.7 | **1.0** | 9.0 | 1-Butene | 0.4 | 1.9 | 0.6 | **3.6** |
| 1,3-Butadiene | 0.1 | 0.6 | **0.7** | 0.4 | trans-2-Pentene | 0.0 | 0.1 | 0.6 | **2.2** |
| trans-2-Pentene | 0.0 | 0.1 | **0.6** | 2.2 | 1-Pentene | 0.1 | 0.4 | 0.2 | **0.9** |
| 1-Butene | 0.4 | 1.9 | **0.6** | 3.6 | Methacrolein | 0.7 | 2.7 | 0.2 | **0.7** |